



Published in final edited form as:

J Am Chem Soc. 2009 October 28; 131(42): 15358–15374. doi:10.1021/ja9058958.

Mechanism of Amido-Thiourea Catalyzed Enantioselective Imine Hydrocyanation: Transition State Stabilization via Multiple Non-Covalent Interactions

Stephan J. Zuend and Eric N. Jacobsen

Harvard University, Department of Chemistry & Chemical Biology, Cambridge, MA 02138.

jacobsen@chemistry.harvard.edu

Abstract

An experimental and computational investigation of amido-thiourea promoted imine hydrocyanation has revealed a new and unexpected mechanism of catalysis. Rather than direct activation of the imine by the thiourea, as had been proposed previously in related systems, the data are consistent with a mechanism involving catalyst-promoted proton transfer from hydrogen isocyanide to imine to generate diastereomeric iminium/cyanide ion pairs that are bound to catalyst through multiple non-covalent interactions; these ion pairs collapse to form the enantiomeric α -aminonitrile products. This mechanistic proposal is supported by the observation of a statistically significant correlation between experimental and calculated enantioselectivities induced by eight different catalysts ($P \ll 0.01$). The computed models reveal a basis for enantioselectivity that involves multiple stabilizing and destabilizing interactions between substrate and catalyst, including thiourea-cyanide and amide-iminium interactions.

Introduction

Catalysis by neutral, organic, small molecules capable of binding and activating substrates solely via non-covalent interactions—particularly H-bonding—has emerged as an important approach to enantioselective synthesis over the last decade.¹ The mechanisms by which such small-molecule catalysts induce high enantioselectivity may be quite different from those employed by catalysts that rely on covalent interactions with substrates. The latter – typified by chiral Lewis acids,² transition metal complexes,³ and secondary amine derivatives⁴ – are generally understood to induce enantioselectivity through steric destabilization of all but the dominant pathway. Repulsive steric effects are strongly distance-dependent,⁵ and expected to be most pronounced in covalently-bound intermediates and transition states. Attractive non-covalent interactions are weaker, less distance-dependent, less directional, and more affected by entropy than covalent interactions.⁶ This analysis defines the challenge for achieving high enantioselectivity through non-covalent interactions alone: the attractive non-covalent interaction (e.g., H-bonding) that binds the enantioselectivity-determining transition structure to the catalyst may be substantially less distance-dependent than the repulsive steric interactions needed to disfavor competing pathways. If that is the case, then the penalty of avoiding repulsive steric interactions by structural reorganization should be relatively small.

Correspondence to: Eric N. Jacobsen.

Supporting Information Available: Complete experimental procedures, characterization data, ¹H NMR spectra used in isotopic labeling and isotope effect experiments, kinetic data in tabular format, geometries and energies of calculated stationary points, computed harmonic frequencies used in isotope effect calculations, and complete ref⁵⁶. This material is available free of charge via the Internet at <http://pubs.acs.org>.

However, the conformational constraint required for high stereoselection may be achieved, in principle, if *multiple* non-covalent attractive interactions are operating in concert. Enzymes engage such cooperative effects as a general principle,^{7,8} and we are interested in exploring the extent to which the interplay of weak, non-covalent interactions is also important in highly selective reactions promoted by small molecule catalysts.⁹

The urea- and thiourea-catalyzed enantioselective hydrocyanation of imines are important examples of small-molecule catalyzed reactions thought to involve only non-covalent substrate-catalyst interactions (Scheme 1).¹⁰ In 2002, a preliminary mechanistic analysis of this reaction – based on NMR spectroscopic, kinetic, structure-activity, and theoretical studies – revealed that the urea functionality of **1b** is responsible for catalytic activity and that the imine substrate engages in a ground-state interaction with the catalyst via a dual H-bonding interaction to the urea protons (Figure 1).¹¹ This study helped to establish that simple H-bond donors could serve as useful chiral small-molecule catalysts, and laid the foundation for much of the subsequent work in this field.¹ However, the mechanism of catalysis, and specifically the question of whether the H-bonding interaction between imine and (thio)urea persisted in the rate- or enantioselectivity-determining transition state, could not be elucidated on the basis of this study.

It was discovered subsequently that urea and thiourea derivatives engage a variety of weakly basic electrophiles, including *N*-acyl iminium/chloride¹² and oxocarbenium/chloride ion pairs,¹³ in catalytic asymmetric reactions. On the basis of substituent and solvent effects, as well as the well-known anion-binding properties of ureas and thioureas,¹⁴ this work led to the proposal that catalysis occurs by abstraction of an anionic leaving group (e.g., Cl⁻) (Scheme 2).^{12b,15}

The notion that multiple mechanistic channels are available to (thio)urea derivatives in catalysis of nucleophile-electrophile addition reactions—and specifically that H-bonding may occur either directly to the electrophile or to an anionic counterion or nucleophile in the enantioselectivity-determining transition structure—has emerged from theoretical studies of reactions promoted by tertiary amino-thiourea derivatives.¹⁶ For example, in the thiourea-catalyzed cyanosilylation of ketones, relatively small differences in activation energy were calculated between mechanisms involving thiourea-ketone and thiourea-cyanide interactions (Scheme 3).^{16c} Analogous considerations may apply to imine hydrocyanation reactions, raising the possibility that the thiourea-imine interactions identified in the preliminary mechanistic work might lie off the productive catalytic cycle.

The mechanism of imine hydrocyanation has been subjected to rigorous scrutiny in the context of non-asymmetric methods, whereas current understanding of enantioselective catalytic variants is more qualitative. Hydrocyanation of imines is promoted by polar, protic solvents such as methanol, but proceeds slowly in non-polar or aprotic solvents, and is inhibited under basic conditions.^{17,18} Insight into the timing and precise mechanism of the σ -bond formation and protonation steps is available from classical studies of nucleophilic additions to carbonyl and imine electrophiles conducted on reactions run in aqueous or alcoholic media.^{19,20} Under these conditions, solvent molecules can assist in proton transfer steps that may be required for reaction.²¹ Indeed, experimental and theoretical studies of non-asymmetric imine hydrocyanation have led to the proposal that solvent molecules (e.g., water or methanol) participate in charge separation and promote proton transfer from HCN to the imine, resulting in the formation of a highly reactive iminium/cyanide ion pair that collapses to afford the α -aminonitrile product (e.g., Scheme 4A).^{22,23} In contrast, asymmetric catalysis of imine hydrocyanation by chiral Lewis or Brønsted acids is generally most effective in non-polar, aprotic solvents, such as toluene.²⁴ Solvent-mediated proton transfer is not possible under these conditions, and most mechanistic proposals for asymmetric imine hydrocyanation invoke direct interactions between imine and Lewis or Brønsted acid (e.g., Scheme 4B),²⁵ rather than

formation of an iminium/cyanide ion pair. In these cases, protonation is proposed to occur after nucleophilic addition,^{25a,b} or by the catalyst itself.^{25c,d,e} The mechanisms proposed until now for non-asymmetric and asymmetric imine hydrocyanation are therefore fundamentally different,²⁶ and bear close parallels to the two limiting mechanisms outlined in Scheme 3 for thiourea catalysis of ketone cyanosilylation.

In this paper we describe a detailed experimental and computational study of highly enantioselective imine hydrocyanation reactions catalyzed by recently discovered urea and thiourea derivatives. We have found that the mechanism of thiourea-catalyzed imine hydrocyanation does not involve productive thiourea-imine interactions (Figure 1); instead, all data are consistent with a mechanism in which imine protonation by hydrogen cyanide precedes nucleophilic addition (e.g., as in the water-mediated reaction, Scheme 4A). This study has identified a role for each functional group on the chiral catalyst, and has revealed a basis for catalysis and enantioinduction that involves multiple stabilizing electrostatic interactions between catalyst and the bound iminium and cyanide ions.

Results and Discussion

A. Identification of a simplified hydrocyanation catalyst

Our efforts to carry out detailed investigations of imine hydrocyanation reactions catalyzed by thiourea Schiff base catalysts such as **1a–c** were limited severely by the structural complexity of the catalysts. However, we discovered recently that *N*-benzhydryl imines (**2**) undergo highly enantioselective imine hydrocyanation with the much simpler amido-thiourea catalyst **4a** (Table 1).²⁷ This reaction displays broad substrate scope, with aldimines bearing either sp³- or sp²-hybridized substituents undergoing hydrocyanation in high yield and enantioselectivity (entries 1–7). Urea-analogue **4b** promotes hydrocyanation to afford α -aminonitriles in similar enantiomeric excess and yield as thiourea **4a** (entries 8–10). This observation indicates that these catalysts operate by similar mechanisms as H-bond donors, and that the nucleophilicity at sulfur of the thiourea catalyst **4a** does not play a direct role in the catalytic mechanism.

B. Kinetic studies of (Thio)urea-catalyzed imine hydrocyanation

In order to establish the stoichiometry of the rate-limiting transition structure, we carried out a detailed kinetic analysis of the imine hydrocyanation reaction catalyzed by **4a**. Rate studies were executed using representative substrate **2a** at synthetically relevant concentrations using in situ infrared spectroscopy. The kinetic experiments were executed under homogeneous conditions, in which HCN was generated in situ by addition of controlled amounts of MeOH to solutions of TMSCN in toluene.²⁸ Data obtained from eighteen independent experiments over a range of concentrations of HCN (0.06–0.35 M), **2a** (0.01–0.15 M), and catalyst **4a** (0.00080–0.0064 M) were used to derive an empirical rate law for the reaction. Kinetic modeling of the experimental data reveals good agreement with the rate law given by eq 1 (Figures 2 and 3):^{29,30,31}

$$\begin{aligned} \text{rate} &= k[\text{HCN}]^a[\text{imine}]^b[\text{cat}]_{\text{tot}}^c; \\ k &= 0.58 \pm 0.02 \text{ M}^{-2} \text{ s}^{-1}, a = 1.09 \pm 0.02, b = 1.06 \pm 0.01, c = 0.812 \pm 0.007 \end{aligned} \quad (1)$$

The values of the exponents *a* and *b* are both approximately 1, and thus analysis of the data reveals an approximately first-order dependence of rate on both [HCN] and [imine]. In contrast, the value of *c* is somewhat less than 1, and the deviation from unity in the rate dependence on [cat]_{tot} appears to be statistically significant.

We considered different possible explanations for the deviation from a strict first-order dependence of rate on $[\text{cat}]_{\text{tot}}$. (a) The deviation from first-order kinetics might be explained by irreversible catalyst deactivation. “Same excess” experiments³² were carried out in order to establish whether consistent kinetic behavior (i.e., the same rate law) was maintained throughout the course of the entire reaction. The perfect overlap of kinetic runs executed at different ratios but same excess of $[\text{HCN}]$ relative to $[\text{imine}]$ (compare red and blue points in Figure 2) reveals that no significant catalyst deactivation occurs, and that product inhibition is insignificant.³³ (b) In principle, the deviation from first-order kinetics might also be explained by competitive uncatalyzed imine hydrocyanation under the reaction conditions. However, the initial rate of the uncatalyzed reaction is approximately 5% of the initial rate of the reaction using the lowest catalyst concentration (0.00080 M). In addition, the enantiomeric ratio is independent of $[\text{cat}]_{\text{tot}}$ under the conditions used in the kinetic analysis (13:1–14:1 er). Both observations indicate that uncatalyzed background reaction is negligible under the conditions of the kinetic analysis. (c) Having ruled out other possible explanations for this effect, we ascribe the small deviation from a first-order rate dependence on $[\text{cat}]_{\text{tot}}$ reversible formation of an inactive catalyst dimer at high $[\text{cat}]_{\text{tot}}$.^{34,35} However, it is important to note that this effect is small and that the precise origins of this effect do not appear to have any bearing on the mechanism of catalysis or enantioinduction, as the enantiomeric excess of the product is the same at different catalyst concentration (vide supra).

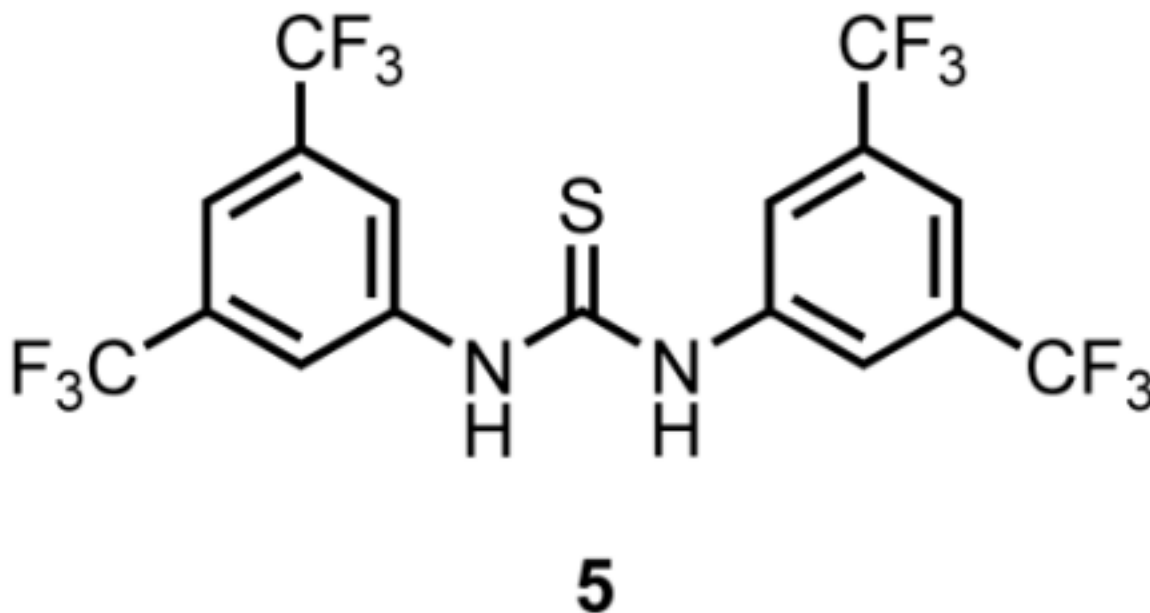
The kinetic data do not distinguish between the two fundamentally different mechanisms in Scheme 5: (a) protonation of the imine to form a transient iminium ion, followed by nucleophilic addition of cyanide anion to form the α -aminonitrile product (Scheme 5A);^{36,37} or (b) addition of cyanide to an imine to form an α -amidonitrile anion, followed by protonation to form the α -aminonitrile product (Scheme 5B). In order to evaluate the relative timing of the protonation and cyanide addition steps in the thiourea-catalyzed imine hydrocyanation reaction, we sought to assess the sense and degree of charge development at the imine-derived nitrogen in the rate-determining transition state. The first-order dependence on both $[\text{imine}]$ and $[\text{HCN}]$ observed experimentally indicates that the imine reactant is not associated with HCN or catalyst in the resting state. Thus a mechanism that involves rate-limiting formation of an iminium ion intermediate (e.g., step 1 in Scheme 5A) will be characterized by an increase in positive charge at nitrogen and faster rates are expected with substrates that better stabilize that positive charge. In contrast, a mechanism that involves an α -amidonitrile intermediate is expected to be characterized by faster rates with substrates that better stabilize negative charge. To distinguish between these possibilities, we measured the rates of hydrocyanation of substituted benzaldehyde-derived imines promoted by thiourea catalyst **4a** and urea analogue **4b** (Figure 4).³⁸ Hammett plots reveal negative ρ -values that are similar in magnitude ($\rho_{\text{thiourea}} = -2.7 \pm 0.2$; $\rho_{\text{urea}} = -2.5 \pm 0.2$),³⁹ consistent with substantial positive charge buildup in the transition state compared with the imine reactant.^{40,41,42} These data provide compelling evidence against the involvement of an α -amidonitrile anion (Scheme 5B) in the (thio)urea-catalyzed imine hydrocyanation, and point instead to an iminium ion mechanism (Scheme 5A).^{43,44}

Schreiner’s achiral thiourea (**5**)⁴⁵ is also an efficient catalyst for hydrocyanation of imine **2a**. Kinetic analysis under conditions similar to those used with chiral catalyst **4a** affords an adequate fit to eq 2:⁴⁶

$$\text{rate} = k[\text{HCN}][\text{imine}][\text{cat}]_{\text{tot}} \quad k = 1.205 \pm 0.008 \text{ M}^{-2} \text{ s}^{-1} \quad (2)$$

A Hammett study of the hydrocyanation catalyzed by **5** reveals that electron-rich substrates react more rapidly than electron-poor ones (Figure 5), as is the case for reactions catalyzed by

chiral catalysts **4a** and **4b**. The derived ρ value of -3.3 ± 0.1 is slightly larger than in the enantioselective reactions, indicating that imine hydrocyanation catalyzed by **5** involves a somewhat greater degree of positive charge buildup than imine hydrocyanation catalyzed by **4a** or **4b**. Nonetheless, because the kinetic behavior and ρ values in imine hydrocyanation reactions catalyzed by **4a** and **5** are similar, it appears reasonable to conclude that these catalysts promote hydrocyanation by analogous mechanisms.⁴⁷



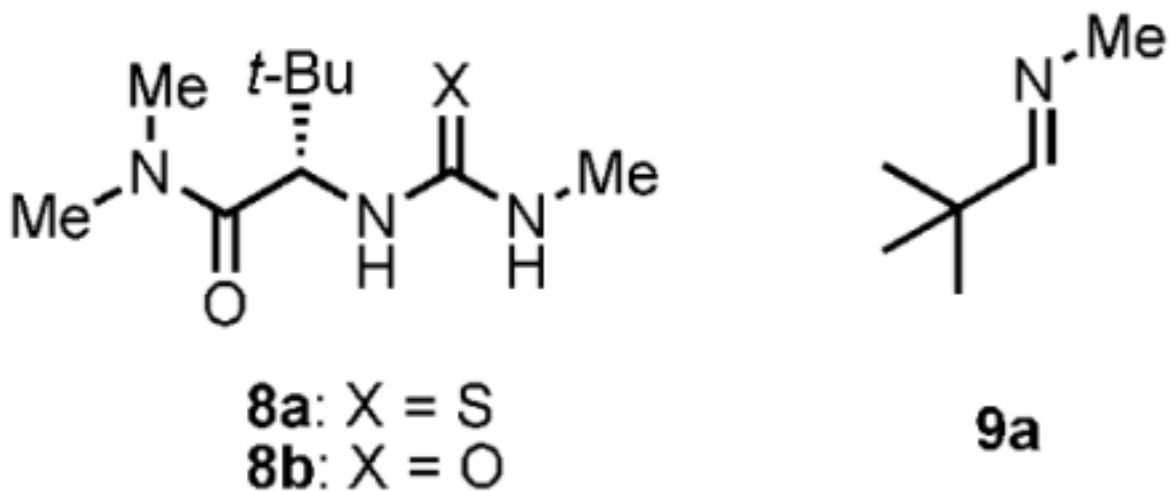
C. Correlation between catalyst structural properties and reaction rate and enantioselectivity

The rate of imine hydrocyanation is only slightly lower with Schreiner's catalyst (**5**) than with the chiral amidothiourea **4a** (compare Figures 4 and 5, or data in the Supporting Information), indicating that an H-bond donor alone is sufficient for efficient catalysis of this reaction.⁴⁸ In order to glean insight into the mechanism of stereoinduction in the asymmetric reaction, the impact of catalyst structural properties on the rate and enantioselectivity of hydrocyanation of imine **2a** was assessed by a combination of kinetic analysis using in situ IR spectroscopy and ee determinations using chiral HPLC analysis.⁴⁹ Analysis of the data indicates that replacing the 3,5-bis-trifluoromethylanilino group with less electron-deficient anilines leads to a substantial decrease in activity without substantial change in enantioselectivity (Table 2.2, entries 1–3). Urea-derived catalyst **4b** is slightly less active and enantioselective than **4a** (entries 1 and 4). In contrast, altering the properties of the amino acid-derived portion of the catalyst leads to substantial decreases in both activity and enantioselectivity (entries 1, 5–10). The (*R*)-enantiomer is the major product in reactions promoted by (*S*)-amino acid-derived catalysts in all but one case (entry 8).⁵⁰ The observation that catalyst **4a** is both the most enantioselective and the most reactive catalyst identified in this series raises the possibility that the stereochemical outcome of the reaction is a result of not only selective destabilization of the transition state leading to the minor (*S*)-enantiomer, but also of selective stabilization of the transition state leading to the major (*R*)-enantiomer.

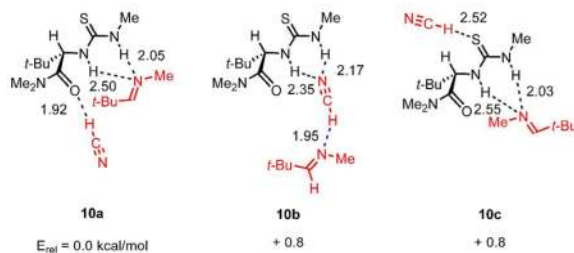
D. Consideration of limiting mechanisms for thiourea-catalyzed imine hydrocyanation: computational studies with a simplified model system

The kinetic and mechanistic analyses described above indicate that thiourea-catalyzed imine hydrocyanation is accompanied by positive-charge buildup on the imine, and likely involves the intermediacy of an iminium ion. The structure-activity-enantioselectivity relationship data provide qualitative information about the critical features of the catalyst, revealing for example that the structures of both the amide and the amino-acid derived portion of the catalyst are critical for both enantioselectivity and activity. In principle, further information about substrate-catalyst interactions might be obtained from spectroscopic or crystallographic analyses of substrate-catalyst complexes. However, such complexes are expected to be weakly bound, and the rates of formation and dissociation of such complexes will almost certainly be much greater than the rate of the catalytic reaction.⁵¹ Under these conditions, spectroscopic analyses are unlikely to provide insight into interactions that occur in transition states.^{52,53}

In contrast, computational chemistry is well-suited to the characterization of complex transition states in organic chemical reactions,⁵⁴ including in the context of asymmetric organocatalysis.⁵⁵ We thus turned to computational methods to obtain deeper insight into the reaction mechanism and to identify catalyst-substrate interactions responsible for catalysis and asymmetric induction.⁵⁶ Catalyst **8a** and model substrate **9a** have limited conformational flexibility, were therefore selected as starting points for comparing energies of a variety of transition structures. Initial calculations were executed at the B3LYP/6-31G(d) level, and all energies refer to uncorrected electronic energies at this level of theory, unless noted otherwise. To test the validity of using this computational method, key transition structures were recalculated at the MP2/6-31G(d) and M05-2X/6-31+G(d,p) levels.⁵⁷



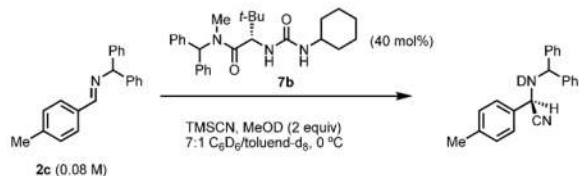
To establish a reference point for analysis of transition structures, ternary complexes of imine, HCN, and catalyst were identified. Complexes **10a-c** involving either thiourea-cyanide or thiourea-imine interactions are each stabilized by three hydrogen bonds and were found to be nearly isoenergetic.



1) Addition of hydrogen cyanide to thiourea-bound imine—One possible mechanism for imine hydrocyanation involves direct imine activation by catalyst via an imine–thiourea complex.¹¹ Within such a mechanism, a possible role of the amide might be to activate HCN or HNC to generate a more active nucleophile.^{25b} Transition state calculations indicate that a mechanism involving a combination of amide–HNC and thiourea–imine interactions has a high activation barrier but is viable (Scheme 6). Because this mechanistic proposal suggests a direct role for the amide, it might also help explain the strong effect of amide structure on reaction rate and enantioselectivity. The computational analysis reveals that proton transfer from one of the *N*-protons of the thiourea occurs to the imine nitrogen simultaneously with cyanide addition.⁵⁸ This proton transfer would be expected to lead to positive charge development on the imine in the rate-limiting transition structure and therefore appears to be consistent with the results of the Hammett analysis (Figure 4).

However, both rate data comparing the urea and thiourea catalysts and isotopic labeling data allow us to rule out the mechanism in Scheme 6. Thioureas are more acidic than ureas by approximately 6 pKa units, and this difference in acidity holds across a broad range of substitution patterns.⁵⁹ If the thiourea or urea catalyst undergoes deprotonation prior to or during the rate-limiting step, then thiourea **4a** is expected to be substantially more active than urea **4b**. Indeed, the computational analysis of the thiourea-bound-to-imine mechanism (Scheme 6) predicts that the activation energy for the urea-catalyzed reaction is 5.3 kcal/mol greater than for the thiourea-catalyzed reaction.⁶⁰ However, this effect is not borne out experimentally: **4a** catalyzes imine hydrocyanation of a range of substrates only slightly more rapidly than **4b** (2–3-fold, see Figure 4 and Table 2).

In the thiourea-bound-to-imine mechanism (Scheme 6), a thiourea proton is incorporated into the α -aminonitrile product.^{25c,d,e} Identification of the origin of the *N*-proton in the α -aminonitrile product would therefore provide a straightforward test of the plausibility of this mechanistic proposal. Amido-urea derivative **7b** was identified as an efficient and enantioselective imine hydrocyanation catalyst in which the urea *N*–H resonances could be monitored by ¹H-NMR spectroscopy under the catalytic reaction conditions. When deuterium cyanide rather than hydrogen cyanide is used as a cyanide source, exchange of the *N*-protons of **7b** occurs slowly, both in the absence and presence of imine. Hydrocyanation of imine **2c** proceeds more rapidly than hydrogen/deuterium exchange, and nearly quantitative deuterium incorporation into the α -aminonitrile product is observed by ¹H-NMR spectroscopy well before one catalytic turnover is reached (eq 3 and Figure 6). Under these conditions, only small amounts of exchange between the urea *N*-protons and DCN are observed (compare the integration of the *N*-protons in Figures 6A, 6B, and 6C).⁶¹ These observations lead to the conclusion that the source of the *N*-proton on the α -aminonitrile is HCN rather than catalyst, and this is inconsistent with the mechanism depicted in Scheme 6. It is thus necessary to consider alternative mechanistic possibilities for imine hydrocyanation.⁶²



(3)

2) Addition of cyanide to catalyst-bound iminium ion—As discussed above, the proposed mechanism for water-mediated imine hydrocyanation involves proton transfer from HCN to imine to form an iminium/cyanide ion pair, followed by collapse to form the α -aminonitrile product (Figure 2A).²² We considered the possibility that chiral amido-thiourea catalysts might promote hydrocyanation via an analogous mechanism. The computational analysis depicted in Scheme 7 indicates that HCN-mediated imine hydrocyanation can proceed by thiourea-assisted proton transfer from HCN to imine to form a transient catalyst-bound ion pair that collapses to form the α -aminonitrile product (**A** \rightarrow **C**). The iminium ion in the transition structure (**B**) is stabilized by a tight H-bond to the amide moiety of the catalyst, whereas the cyanide anion is stabilized by a dual H-bond to the thiourea moiety of the catalyst. The computational analysis with this simplified catalyst suggests that this process is formally concerted but highly asynchronous: the C–H bond between cyanide and iminium ion is partially broken in the transition structure, but almost no C–C bond formation has occurred at this point on the reaction coordinate. The reaction coordinate with this simplified model involves rate-limiting proton transfer followed by barrierless cyanide addition.

An analogous mechanism that uses hydrogen isocyanide (HNC) as the active nucleophile was also identified by computational methods (Scheme 8).⁶³ This mechanism for imine hydrocyanation involves two discrete steps. The first step (**A** \rightarrow **C**) involves proton transfer from HNC to imine to generate a catalyst-bound iminium/cyanide ion pair (**C**). In order for the cyanide anion to be able to approach the iminium ion in a Bürgi-Dunitz trajectory,⁶⁴ further charge and spatial separation is necessary. The rate-limiting step in the overall transformation involves structural reorganization of this ion pair to form a transition structure with a long forming C–C bond that collapses to the α -aminonitrile (**C** \rightarrow **E**). The overall activation barrier for HNC addition is slightly lower than for HCN addition. However the key stabilizing substrate-catalyst interactions in the transition structures (Schemes 7B and 8D) are nearly identical: both transition structures involve a network of medium-length H-bonds between cyanide and thiourea (1.9–2.2 Å), between iminium and cyanide (2.1–2.2 Å), and between amide and iminium ion (2.2 Å).⁶⁵ Because of the overall similarities between these mechanistic hypotheses, and the limited relevance of the simplified model system used in this study, we have not made further efforts to distinguish between these pathways.⁶⁶

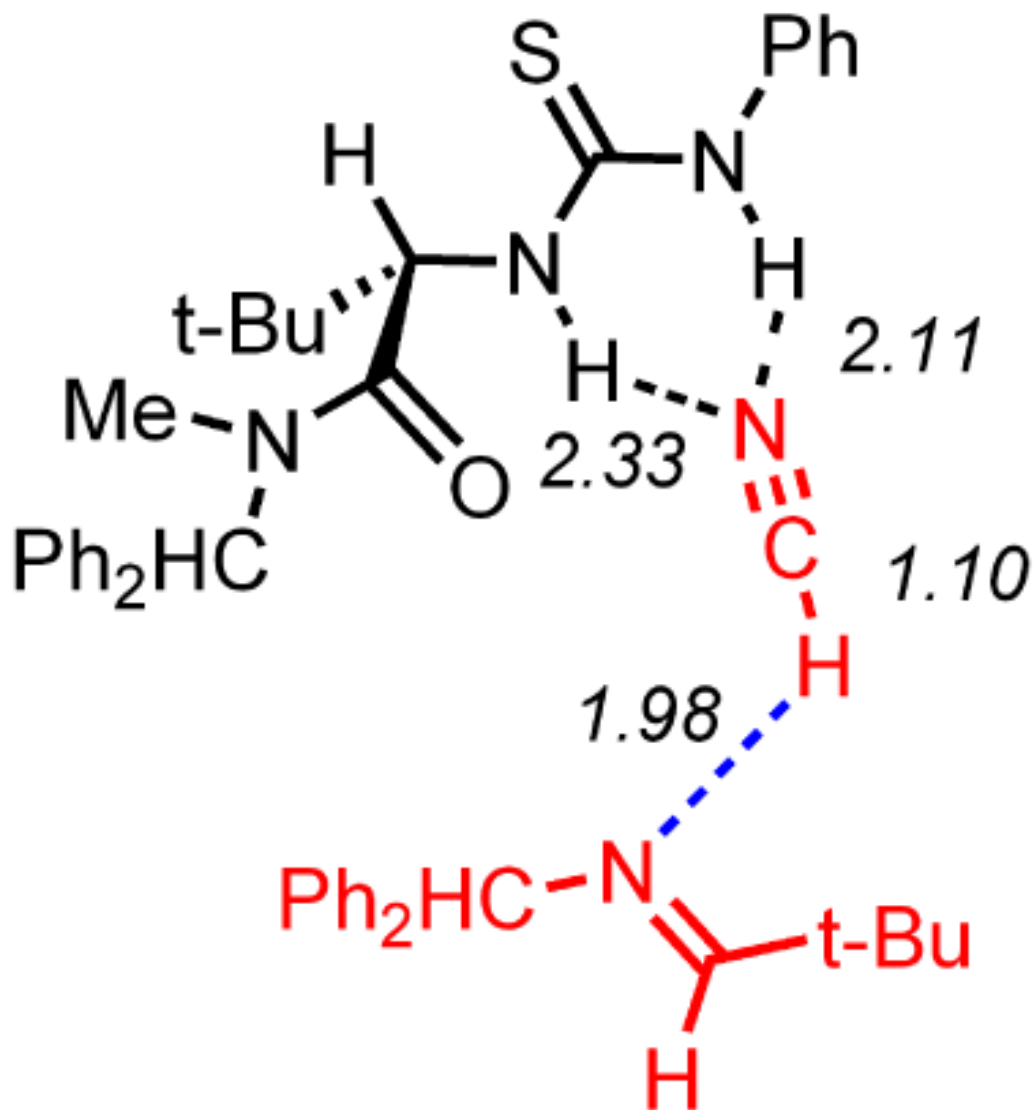
The mechanistic hypothesis that either HCN or HNC protonates the imine to generate a catalyst-bound ion pair (Schemes 7 and 8) is consistent with the experimental data: (a) each of the proposed mechanisms involves positive-charge buildup on the imine, and is thus consistent with the Hammett analysis; (b) each proposed mechanism involves imine protonation by the nucleophile rather than the catalyst, and is thus consistent with the experimental observation that α -aminonitrile *N*-proton originates from the nucleophile rather than from the catalyst. In addition, the overall calculated activation barrier for hydrocyanation via an iminium/cyanide ion pair is 20 kcal/mol lower than hydrocyanation by direct addition to a catalyst-bound imine.⁶⁷

The HCN- and HNC-addition transition structures leading to the (*R*)- and (*S*)-enantiomers of α -aminonitrile are depicted in Figures 7 and 8. Each of the two sets of structures differs with respect to the orientation of the substrate *tert*-butyl group relative to the catalyst, but both possess the same cyanide-thiourea and iminium-amide interactions. The HCN- and HNC-addition transition structures leading to each enantiomer of product are remarkably similar, and differ only in the orientation of the cyanide anion relative to the catalyst and iminium ion. The similarities in the transition structure geometries thus provide an explanation for why transition structures formally originating from tautomeric nucleophiles have such similar energies. Nevertheless, the HNC-addition is more favorable than HCN-addition transition structures in every case examined, and our analysis is therefore focused on HNC-addition mode for the remainder of this paper.⁶⁸

Calculations of the HNC-addition transition structures—including full geometry optimizations—at the M05-2X/6-31+G(d,p) and MP2/6-31G(d) levels yield nearly identical transition structures and relative energies (Supporting Information). This mechanistic proposal is thus consistent with the experimental data, and the geometries of the transition structures are consistent across different theoretical methods; we thus conclude that an imine hydrocyanation mechanism involving a catalyst-bound iminium/cyanide ion pair is viable. However the simplified model system examined in this study does not serve to address the high enantioselectivity observed experimentally in the catalytic reaction.⁶⁹ In order to account for the experimental catalyst structure-activity data (Table 2) and attempt to develop an understanding of the basis of stereinduction, it is necessary to evaluate catalyst and substrate structures that are more relevant to the catalytic, enantioselective reaction.

E. Computational analysis of imine hydrocyanation with substituted amido-thiourea catalysts

A broad range of enantioselectivities are observed in imine hydrocyanation with different amido-(thio)urea catalysts (Table 2), and we sought to determine whether computational methods can be used to account for the observed trends in a quantitative manner.^{70,71} For such an analysis to be meaningful, the computational models must incorporate all the catalyst and substrate structural features necessary for high enantioselectivity. As discussed above, both the identity of the amide and the amino acid components play crucial roles in defining the enantioselectivity of the catalyst. In contrast, the precise structure of the anilino group has little effect on enantioselectivity (Table 2, entries 1–3), so we selected the simple phenyl-substituted catalyst **6a**, together with an imine that undergoes hydrocyanation with high ee, *N*-benzhydryl imine **2a**, for our model. In the following discussion, energies of all calculated intermediates and transition structures are provided relative to the stable complex between catalyst, substrate, and HCN shown below.



$$E = 0 \text{ kcal/mol}$$

Scheme 9 provides a representation of the calculated intermediates and transition states in the lowest energy pathway for the addition of HNC to imine **2a** catalyzed by thiourea **6a**. The first two steps of this mechanism (**A** → **C** → **E**) involve formation of a catalyst-bound iminium-cyanide ion pair. This ion pair then undergoes structural rearrangement to form new ion pair in which the iminium ion is associated to the amide component of the catalyst (**E** → **G**). In this model system, there is a small barrier calculated for the collapse of this ion pair to form the (*R*)- α -aminonitrile product (**G** → **I**). As with the simpler model system described above, the highest energy transition state, and therefore the rate-limiting step, is associated with the ion pair reorganization step (compare Scheme 8, **C** → **E** with Scheme 9, **E** → **G**). In short, the basic calculated HNC-mediated imine hydrocyanation mechanisms are predicted to correspond

closely in the small and large model systems; the mechanisms differ only in the number of intermediates and transition structures that are observed prior to and after the rate-limiting step.

An analogous computational analysis of the formation of the (*S*)- α -aminonitrile yields a similar reaction coordinate (Supporting Information), in which a transition structure akin to **F** is predicted to represent the rate-limiting step ($E = +19.4$ kcal/mol). The calculated relative energies of the ion pair rearrangement transition structures ($\Delta\Delta E^\ddagger = 2.4$ kcal/mol) thus correspond well with the experimentally observed preference for formation of the (*R*)- α -aminonitrile. This analysis assumes that the calculated rate-limiting step, **E** \rightarrow **G**, is enantioselectivity-determining. It is important to note that the calculations also predict the same sense and similar magnitude of enantioselectivity if the cyanide-addition step, **G** \rightarrow **I**, is enantioselectivity-determining. Thus comparison of the energies of transition structure **H** (Scheme 9) and the corresponding structure leading to the (*S*)- α -aminonitrile (Supporting Information) also reveals a significant preference for formation of (*R*)- α -aminonitrile ($\Delta\Delta E^\ddagger = 2.1$ kcal/mol). The computational analysis therefore provides support for either iminium-ion rearrangement or cyanide addition as enantioselectivity-determining steps in the catalytic reaction, although it predicts a higher barrier to the former.

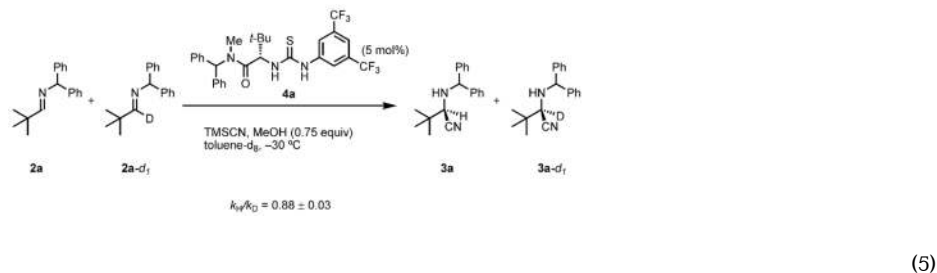
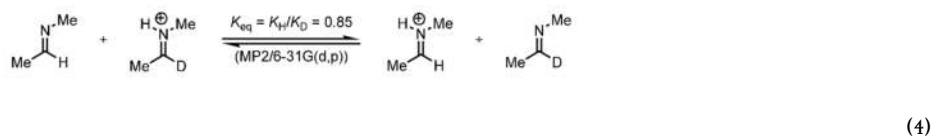
F. Secondary kinetic isotope effect experiments

We explored alternative approaches to establish the identity of the enantioselectivity-determining step with greater certainty. In principle, the question of which of transition structures **F** and **H** in Scheme 9 is rate-determining might be addressed by examining secondary isotope effects in the hydrocyanation reaction. A key difference between these transition structures is that **H** undergoes partial $sp^2 \rightarrow sp^3$ rehybridization of the electrophilic carbon atom, whereas **F** does not. Secondary α -hydrogen/deuterium kinetic isotope effects (KIEs, k_H/k_D) are sensitive probes of changes in carbon hybridization state,⁷² and inverse α -KIEs are observed in reactions thought to involve significant $sp^2 \rightarrow sp^3$ rehybridization (typically, $k_H/k_D \approx 0.75 - 0.90$).⁷³

However, in reactions of carbonyl derivatives that involve reversible protonation or Lewis acid complexation of the carbonyl prior to nucleophilic addition, it is also necessary to consider secondary β -hydrogen/deuterium equilibrium isotope effects (EIEs) on lone pair basicity.⁷⁴ Accurate and systematic measurements of β -EIEs on nitrogen basicity have been reported only recently, and these studies have revealed that β -deuterium substituted amines are more basic than their β -protio analogues in aqueous solution.⁷⁵ By extrapolation of the experimental data, a maximum β -EIE on basicity of ≈ 46 cal/mol is predicted when the C–H or C–D bond is anti-periplanar to the basic nitrogen ($K_H/K_D = 0.93$ at 298 K).⁷⁶ This effect is reproduced using harmonic frequency calculations at the MP2/6-31G(d,p) level ($K_H/K_D = 0.91$).⁷⁷ C–H stretching frequencies involving sp^2 -hybridized carbons are affected by the presence of an anti-periplanar lone pair,^{74,78} because secondary isotope effects can arise any time a vibrational mode is perturbed in the course of a reaction, an EIE might be expected in imine protonation as well.

To test this notion, we calculated the EIE for protonation of a model imine at the MP2/6-31G(d,p) level using harmonic frequency calculations (eq 4).^{79,80} This analysis predicts a significant inverse EIE on imine basicity comparable in magnitude to the inverse EIE observed experimentally on tertiary amine basicity. Thus the direction of the secondary β -EIE on imine basicity is expected to be the same as the direction of the secondary α -KIE in a reaction involving $sp^2 \rightarrow sp^3$ rehybridization in the transition state. In the asymmetric imine hydrocyanation, an inverse KIE of $k_H/k_D = 0.88 \pm 0.03$ is observed (eq 5).⁸¹ An isotope effect of this magnitude allows us to rule out a late transition state involving a largely sp^3 -hybridized electrophilic carbon,⁷³ but it is consistent with a transition state that involves either early C–C bond formation or iminium ion rearrangement.⁸² Therefore, the experimental secondary

isotope effect data are consistent with either **F** or **H** (Scheme 9) as the rate- and enantioselectivity-determining transition structures. Given that the calculations predict a very low barrier for the cyanide addition step (**G** → **I**), we proceeded in our analysis with the assumption that the iminium ion rearrangement (**E** → **G**) is enantioselectivity-determining.



G. Correlation between experimental and calculated enantioselectivity

The experimental enantioselectivity data listed in Table 2 reveal a strong impact of relatively small changes in catalyst structure on enantioselectivity in the hydrocyanation of **2a**.⁸³ Diastereomeric transition structures akin to **F** depicted in Scheme 9 for addition of HNC to imine **2a** were calculated at the B3LYP/6-31G(d) level for a series of catalysts. Experimental data listed in Table 2 from reactions run with catalysts **4a–4h** were compared with calculations executed using the *N*-phenyl catalysts **6a–6h** (Figure 9). A plot of the relative energies of the (*S*)- and (*R*)-transition structures versus the energy difference between (*S*)- and (*R*)-transition states calculated from experimental ee measurements yields a strong correlation and a statistically significant positive slope (Figure 10).⁸⁴ Single-point energy calculations at the M05-2X/6-31+G(d,p) and MP2/6-31G(d) levels result in similar plots (Figures 11 and 12).^{85,86} Computations at each level of theory reproduce the experimentally observed preference for the (*R*)-enantiomer of product, the higher observed enantioselectivity with **4d** compared with **4e**, the reduced enantioselectivity with secondary amide catalyst **4g** compared with tertiary amide catalyst **4a**, and the preference for the (*S*)-enantiomer of product with catalyst **4f**.⁸⁷

H. Basis for enantioselectivity: the role of cation stabilization

The computational data are strongly consistent with the experimental observation that the enantioselectivity of imine hydrocyanation is strongly dependent on the structure of the catalyst. However, comparison of imine hydrocyanation transition structures using catalysts that induce high enantioselectivity in hydrocyanation (e.g., catalyst **6a**, Figure 13) with those that induce low enantioselectivity (e.g., catalyst **6f**, Figure 14) reveals few obvious differences. In particular, there are no apparent “steric clashes” that might explain why some transition structures are significantly higher in energy than the one leading to (*R*)-**3a** with catalyst **6a**. We therefore undertook a quantitative analysis of structural differences between transition structures using different catalysts. As described below, this analysis has led to the conclusion that enantioselectivity can be attributed primarily to differential stabilization of the iminium cation.

Because imine hydrocyanation is catalyzed by simple H-bond donors (i.e., Schreiner's catalyst, **5**), we considered whether the basis for enantioselectivity might be tied to the dual H-bond interaction between cyanide and (thio)urea. The strength of H-bonds is distance-dependent;⁶ thus, if the cyanide–thiourea H-bond strength changes substantially among the four transition structures, the H-bond lengths in the four transition structures would be expected to be substantially different (d_1 and d_2 in Figure 15). However, the length of the dual H-bond between thiourea and cyanide does not differ substantially amongst the (*R*)- and (*S*)-transition structures with either catalyst: the eight cyanide nitrogen–thiourea proton distances among the four transition structures vary from 1.97 to 2.11 Å (Figures 13 and 14). The small differences in H-bond length among the different structures can be attributed primarily to changes in binding symmetry rather than differences in overall binding strength: the average of the two H-bond lengths of the four structures in Figures 13 and 14 ranges from 2.01–2.05 Å. We reach the same conclusion from a complete analysis of all sixteen HNC-addition transition structures calculated with imine **2a** and catalysts **6a–6g** (Supporting Information). Plots of the sum of the thiourea–cyanide bond lengths ($d_1 + d_2$) versus calculated enantioselectivity reveal that there is no statistically significant trend in H-bond length within either the (*R*)- or (*S*)-transition structures between highly and poorly enantioselective catalysts (Figure 16). Thus, there is no correlation between thiourea–cyanide H-bond length and enantioselectivity, and other explanations must be evaluated for the basis for enantioselectivity.

The calculated rate-limiting step (**E** → **G**, Scheme 9) is rearrangement of an ion pair: in intermediate **E**, the iminium ion forms an H-bond to cyanide anion; in intermediate **G**, the iminium ion forms an H-bond to the oxygen atom of the catalyst carbonyl group. The reaction coordinate thus formally involves transfer of the iminium ion from cyanide to carbonyl, and the transition structure represents a point on the reaction coordinate where the H-bonds from iminium ion to both cyanide (d_3) and amide (d_4) are each partially formed (Figure 17).⁸⁸ A straightforward way to estimate the overall H-bond strength to the iminium ion as the rearrangement proceeds is to measure the sum of the O–H and N–H bond lengths in the HNC-addition transition structures ($d_3 + d_4$).⁸⁹ Plots of the sum of the H-bond lengths versus calculated enantioselectivity reveal that $d_3 + d_4$ varies only slightly across the transition structures leading to the (*R*)-enantiomer (Figure 18). In contrast, there is a positive correlation between $d_3 + d_4$ and enantioselectivity within the (*S*)-transition structures. Comparison of the most and least selective catalysts is striking: whereas $d_3 + d_4$ is significantly different between the (*R*)- and (*S*) addition transition structures with optimal catalyst **6a** (4.58 versus 5.00 Å, Figure 13), this difference is negligible with catalyst **6f** (4.51 Å for both (*R*)- and (*S*)-transition structures, Figure 14). This analysis leads to a simple conclusion: the basis for enantioselectivity may be traced to different degrees of iminium ion stabilization amongst different catalysts and diastereomeric transition structures, and stabilization of the iminium ion is achieved by H-bonding interactions between the iminium ion N–H and both the amide C=O and the thiourea-bound cyanide ion.

Conclusions

This study provides experimental and theoretical support for a mechanism for amido-thiourea catalyzed imine hydrocyanation involving formation of an iminium/cyanide ion pair that is bound to catalyst through multiple non-covalent interactions. This mechanism is analogous to the mechanism proposed for non-asymmetric imine hydrocyanation in polar, protic solvents, in which hydrogen cyanide activates the imine toward nucleophilic attack. In contrast, the data are inconsistent with mechanisms that involve direct imine activation by thiourea. The proposal that a H-bond donor catalyst promotes nucleophilic addition to a basic substrate without a direct interaction between the catalyst's acidic and substrate's basic functional groups may be relevant to catalytic asymmetric nucleophilic additions of other protic nucleophiles.⁹⁰ While stabilization of the cyanide anion by the thiourea is important for catalysis, differences in

enantioselectivity cannot be traced to the degree of anion-stabilization. Instead, we conclude that the degree of stabilization of the iminium ion is principally responsible for controlling enantioselectivity in asymmetric imine hydrocyanation.

Small-molecule organocatalysts promote asymmetric transformations via a variety of fundamentally different activation mechanisms—including covalent catalysis,⁴ general acid-base catalysis,¹⁶ and non-covalent catalysis^{91,92,93}—and these activation modes closely parallel those of enzymatic reactions.⁹⁴ However, small-molecule organocatalysts appear to differ from their macromolecular counterparts in their propensity to bind substrates. The measurement of substrate binding constants is a hallmark of enzymatic kinetic analyses,⁹⁵ and it is a guiding principle in structural biology that the binding orientation of the substrate in an enzyme active site at least partially relevant to the transition structure.⁹⁶ In contrast, kinetically observable substrate binding does not occur in the reaction studied herein, and computational studies suggest that multiple, fundamentally different binding modes are in principle isoenergetic (i.e., complexes **10a–10c**). Imine–urea binding was observed both kinetically and spectroscopically in the context of imine hydrocyanation catalyzed by **1b** (Figure 1),¹¹ but the results described in this paper suggest that this mode of imine binding lies off the productive catalytic cycle.^{97,98,99}

This difference in the relevance of the ground state catalyst-substrate structure to the mechanism of catalysis may be ascribed simply to the structural simplicity of these small-molecule catalysts compared with enzymes. There is no well-defined and structurally rigid “binding pocket” in catalysts such as **4a**; instead, the functional groups necessary for catalysis are exposed to solvent and accessible to a broad range of small molecules, whether or not they are substrates for catalysis. Indeed, the ability of these catalysts to accept many different small-molecules is a prerequisite both for broad substrate scope within any single reaction and for the ability of a single catalyst to promote multiple different reactions. A corollary of this analysis is that enantioselectivity is under Curtin-Hammett control and elucidation of its basis therefore requires detailed understanding of transition structure geometries. The present study demonstrates that weak interactions operating in transition states of polar asymmetric reactions are amenable to quantitative characterization using modern but increasingly inexpensive computational methods.¹⁰⁰ We suggest that systematic application of hybrid experimental-computational approaches such as those described in this paper will prove valuable in the characterization of other enantioselective catalytic processes that rely on non-covalent interactions.

Supplementary Material

Refer to Web version on PubMed Central for supplementary material.

Acknowledgments

This work was supported by the NIH (GM-43214) and by fellowship support to SJZ from the American Chemical Society and Roche. We thank Dr. Lars P. C. Nielsen for helpful discussions.

Notes and References

1. Review, historical perspective, and leading references: Doyle AG, Jacobsen EN. *Chem Rev* 2007;107:5713–5743. [PubMed: 18072808]
2. For classic examples, see: Johnson JS, Evans DA. *Acc Chem Res* 2000;33:325–335. [PubMed: 10891050]
3. Trost BM, Machacek MR, Aponick A. *Acc Chem Res* 2006;39:747–760. [PubMed: 17042475]
4. Recent reviews: (a) Lelais G, MacMillan DWC. *Aldrichimica Acta* 2006;39:79–87. (b) Mukherjee S, Yang JW, Hoffmann S, List B. *Chem Rev* 2007;107:5471–5569. [PubMed: 18072803]

5. For a detailed discussion, see: Israelachvili, J. *Intermolecular & Surface Forces*. Vol. 2. Academic Press; London: 1991. p. 109-121. The strength of repulsive non-bonding interactions is roughly proportional to $(1/r)^{12}$. Within this model, a 25% increase in r leads to a 93% decrease in interaction energy
6. For a tabulation of the orientation- and distance-dependence of attractive non-covalent interactions, see: ref 5, p 28. For example, the strength of a charge-dipole interaction—which approximates the electrostatic component of a hydrogen bond—is proportional to $\cos \theta/r^2$. If the energy of this interaction is 5 kcal/mol when bond length and orientation are optimal, then either a 25% increase in bond length or a 45° rotation of the dipole will cost less than 2 kcal/mol.
7. For a discussion of and leading references to models for enantioselectivity in biological systems, see: Sundaresan V, Abrol R. *Protein Science* 2002;11:1330–1339. [PubMed: 12021432]
8. For leading references to cooperative mechanisms in enzymatic and small-molecule catalysis, see: ref 16c.
9. For a recent discussion of additive effects in supramolecular chemistry, see: Schneider HJ. *Angew Chem, Int Ed* 2009;48:3924–3977.
10. (a) Sigman MS, Jacobsen EN. *J Am Chem Soc* 1998;120:4901–4902. For subsequent studies, see: (b) Sigman MS, Vachal P, Jacobsen EN. *Angew Chem, Int Ed* 2000;39:1279–1281. (c) Vachal P, Jacobsen EN. *Org Lett* 2000;2:867–870. [PubMed: 10754690] (d) Su JT, Vachal P, Jacobsen EN. *Adv Synth Catal* 2001;343:197–200.
11. (a) Vachal P, Jacobsen EN. *J Am Chem Soc* 2002;124:10012–10014. [PubMed: 12188665] See, also: (b) Vachal, P. PhD Thesis. Harvard University; Cambridge, MA: Mar. 2003
12. (a) Taylor MS, Jacobsen EN. *J Am Chem Soc* 2004;126:10558–10559. [PubMed: 15327311] (b) Raheem IT, Thiara PS, Peterson EA, Jacobsen EN. *J Am Chem Soc* 2007;129:13404–13405. [PubMed: 17941641]
13. Reisman SE, Doyle AG, Jacobsen EN. *J Am Chem Soc* 2008;130:7198–7199. [PubMed: 18479086]
14. For a survey of the anion binding properties of ureas and thioureas, see: Sessler, JL.; Gale, PA.; Cho, W-S. *Anion Receptor Chemistry*. RSC Publishing; Cambridge: 2006. p. 193-205.
15. For a review and an analysis of the anion-binding properties of urea derivatives in the context of catalysis, see: Zhang ZG, Schreiner PR. *Chem Soc Rev* 2009;38:1187–1198. [PubMed: 19421588] This paper also contains an up-to-date list of reviews in this area.
16. (a) Hamza A, Schubert G, Soós T, Pápai I. *J Am Chem Soc* 2006;128:13151–13160. [PubMed: 17017795] (b) Hammar P, Marcelli T, Hiemstra H, Himo F. *Adv Synth Catal* 2007;349:2537–2548. (c) Zuend SJ, Jacobsen EN. *J Am Chem Soc* 2007;129:15872–15883. [PubMed: 18052247]
17. (a) Ogata Y, Kawasaki A. *J Chem Soc, B* 1971:325–329. See, also: (b) Taillades J, Commeyras A. *Tetrahedron* 1974;30:127–132. (c) Taillades J, Commeyras A. *Tetrahedron* 1974;30:2493–2501.
18. In contrast, cyanation of carbonyl compounds is subject to basic catalysis: Ching WM, Kallen RG. *J Am Chem Soc* 1978;100:6119–6124. and refs therein
19. Jencks WP. *Chem Rev* 1972;72:705–718.
20. Jencks, WP. *Catalysis in Chemistry and Enzymology*. Dover Publications; New York: 1987.
21. Guthrie JP. *J Am Chem Soc* 1996;118:12886–12890. and refs therein
22. Arnaud A, Adamo C, Cossi M, Milet A, Vallée Y, Barone V. *J Am Chem Soc* 2000;122:324–330.
23. In early studies, it was also proposed that solvent was involved in a proton relay step (i.e., the source of the proton on the α -aminonitrile product is solvent rather than HCN). However, no role for proton relay by water could be identified in ref 22, and water was proposed to promote hydrocyanation through the formation of multiple hydrogen bridges.
24. Recent reviews and leading references: (a) Gröger H. *Chem Rev* 2003;103:2795–2827. [PubMed: 12914481] (b) Nájera C, Sansano JM. *Chem Rev* 2007;107:4584–4671. [PubMed: 17915933] (c) Connon SJ. *Angew Chem, Int Ed* 2008;47:1176–1178.
25. (a) Takamura M, Hamashima Y, Usuda H, Kanai M, Shibasaki M. *Angew Chem, Int Ed* 2000;39:1650–1652. (b) Josephsohn NS, Kuntz KW, Snapper ML, Hoveyda AH. *J Am Chem Soc* 2001;123:11594–11599. [PubMed: 11716713] (c) Li J, Jiang WY, Han KL, He GZ, Li C. *J Org Chem* 2003;68:8786–8789. [PubMed: 14604345] (d) Rueping M, Sugiono E, Azap C. *Angew Chem, Int Ed* 2006;45:2617–2619. (e) Simón L, Goodman JM. *J Am Chem Soc* 2009;131:4070–4077. [PubMed: 19249818]

26. For a recently reported exception to this generalization, see: Negru M, Schollmeyer D, Kunz H. *Angew Chem, Int Ed* 2007;46:9339–9341.
27. Zuend SJ, Coughlin MP, Lalonde MP, Jacobsen EN. *Nature*. Accepted for publication
28. Conversion of TMSCN to HCN could be monitored directly by in situ IR spectroscopy, or indirectly by ¹H-NMR spectroscopy in C₆D₆. Conversion of 2a was determined by monitoring the height of the C=N stretch at 1670 cm⁻¹ relative to a two-point baseline (1570–1770 cm⁻¹).
29. Non-linear least-squares fitting and statistical analysis was executed using SigmaPlot 10.0 purchased from Systat Software.
30. R² = 0.9955 for the fit of the data to eq 1. Details and kinetic data in tabular format are included in the Supporting Information.
31. The kinetic modeling was executed using methods described previously (ref 16c, and refs therein): experimental IR data in the form *absorbance versus time* were first converted to the form *concentration versus time* by application of Beer's Law. These data were converted to the form *rate versus concentration* by least-squares fitting of the *concentration versus time* data to a 7th-order polynomial followed by analytical differentiation of the polynomial. For this approach to be effective, a high data collection rate is necessary, and IR spectra were collected every 15 s for the entire course of the reaction. This approach also requires that the reaction mixture solution be completely homogeneous, and thus IR data collected in the first few minutes after addition of the last reagent are intrinsically inaccurate. In the fastest reactions, there is insufficient data at low %-conversion to apply this approach (i.e., there are too few IR spectra collected within approximately the first 25% conversion to allow for accurate curve fitting). For consistency, all kinetic analyses used data from 25–95% conversion of imine (i.e., [imine] = 0.01–0.15 M where [imine]_i = 0.20 M).
32. Blackmond DG. *Angew Chem, Int Ed* 2005;44:4302–4320.
33. We have only carried out “same excess” experiments at one [cat]_{tot}, and it is possible that at other [cat]_{tot}, some irreversible catalyst deactivation occurs.
34. A fit to a kinetic model that allows for reversible catalyst dimer formation provides an excellent 2 [cat]_{tot} agreement with the experimental data: $rate = k[\text{HCN}][\text{imine}] \frac{2[\text{cat}]_{\text{tot}}}{1 + \sqrt{1 + 8K_{\text{dim}}[\text{cat}]_{\text{tot}}}}$, $k = 1.74 \pm 0.04 \text{ M}^{-2} \text{ s}^{-1}$, $K_{\text{dim}} = 55 \pm 6 \text{ M}^{-1}$, R² = 0.9932. A derivation of this rate law and the corresponding figures are included in the Supporting Information. A fit to $rate = k[\text{HCN}][\text{imine}][\text{cat}]_{\text{tot}}$ provides comparatively poor agreement with the experimental data (see Supporting Information).
35. Aggregation of thiourea catalysts is precedented: (a) ref 16c (b) Tárkányi G, Király P, Varga S, Vakulya B, Soós T. *Chem Eur J* 2008;14:6078–6086. (c) Oh SH, Rho HS, Lee JW, Lee JE, Youk SH, Chin J, Song CE. *Angew Chem, Int Ed* 2008;41:7872–7875.
36. Methanol-mediated racemic imine hydrocyanation proceeds via a mechanism that involves buildup of positive charge on the imine (ρ = -1.1): ref 17a.
37. A concerted [3 + 2] cycloaddition mechanism is also consistent with the kinetic data, and represents an intermediate case. Gas-phase transition structures for a concerted, asynchronous [3+2] cycloaddition between an imine and HNC have been located using both DFT and *ab initio* methods. This process has a calculated activation barrier of 43 kcal/mol. Inclusion of bulk water reduces the calculated activation free energy of the concerted process to 19 kcal/mol. Whereas the gas phase transition structure visually approximates the aqueous transition structure, the latter is characterized by longer breaking N-H and forming C-C bonds, and is more accurately described as an iminium/cyanide ion pair. Explicit inclusion of two water molecules decreases the activation free energy to 16 kcal/mol, and results in a non-concerted, multi-step iminium/cyanide ion pair mechanism: ref 22.
38. Reactions were monitored by sequential removal of aliquots and subsequent ¹H-NMR spectroscopic analysis versus 1,3,5-trimethoxybenzene internal standard. Pseudo first-order rate constants (k_{obsd}) were obtained by a non-linear least squares fit to $f(x) = ae^{-k_{\text{obsd}}x}$. Details and kinetic data in tabular format are provided in the Supporting Information.
39. σ_p values were obtained from: Hansch C, Leo A, Taft RW. *Chem Rev* 1991;91:165–195.
40. A similar ρ value was obtained from a series of competition experiments in imine hydrocyanation reactions catalyzed by 1b (Vachal, P. Unpublished results). To our knowledge, no other Hammett

studies of catalytic asymmetric imine hydrocyanation reactions have been reported; it is thus not possible to establish whether this observation is general.

41. The observed negative ρ -values are large compared with those observed in other reactions of imines. In reactions that involve imine protonation followed by nucleophilic addition (e.g., in imine hydrolysis under non-acidic conditions), the negative Hammett correlation of imine basicity approximately cancels the positive Hammett correlation of iminium ion electrophilicity. Large negative Hammett correlations have been observed for additions for the acid-catalyzed addition of amine nucleophiles to oximes. For a series of classic studies examining substituent effects on imine basicity, see: (a) Cordes EH, Jencks WP. *J Am Chem Soc* 1963;85:2843–2848. (b) Koehler K, Sandstrom W, Cordes EH. *J Am Chem Soc* 1964;86:2413–2419. (c) Archila J, Bull H, Lagenaur C, Cordes EH. *J Org Chem* 1971;36:1345–1347.
42. The observed negative ρ -values are small compared with those of reactions that proceed through a cationic transition structure not stabilized by a heteroatom; e.g., acid-catalyzed hydration of styrene derivatives: Schubert WM, Keeffe JR. *J Am Chem Soc* 1972;94:559–566.
43. The gas phase basicity (proton affinity) of *para*-substituted benzaldehyde-derived imines *N*-H imines was also computed by DFT methods (B3LYP/6-31G(d)). Details are provided in the Supporting Information.
44. A mechanism that involves positive charge buildup on the organic electrophile would likely also involve negative charge buildup on the nucleophile; thus such a mechanism is expected to be characterized by high reaction rates with nucleophiles that are able to stabilize negative charge. The structural simplicity of cyanide anion that renders it ideal for computational analysis (*vide infra*) does not allow a direct test of this hypothesis. However, thiourea-catalyzed asymmetric imine hydrophosphonylation appears to be mechanistically related to imine hydrocyanation, and proceeds most rapidly with electron-deficient phosphites: Joly GD, Jacobsen EN. *J Am Chem Soc* 2004;126:4102–4103. [PubMed: 15053588]The observation that aprotic phosphites are unreactive foreshadows the conclusion that proton transfer from nucleophile precursor to imine precedes nucleophilic addition (*vide infra*).
45. Schreiner PR, Wittkopp A. *Org Lett* 2002;4:217–220. [PubMed: 11796054]
46. Data are included in the Supporting Information. The fit to eq 2 affords $R^2 = 0.980$. A fit to $rate = k [\text{HCN}]^a [\text{imine}]^b [\text{cat}]_{\text{tot}}^c$ affords: $k_{\text{cat}} = 2.8 \pm 0.3 \text{ M}^{-2} \text{ s}^{-1}$, $a = 1.03 \pm 0.04$, $b = 0.97 \pm 0.02$, $c = 1.17 \pm 0.02$, $R^2 = 0.987$.
47. Achiral thiourea 5 catalyzes hydroalkoxylation of electron-rich olefins. The proposed mechanism for this transformation involves olefin protonation followed by alkoxide addition in a formally concerted but highly asynchronous manner: Kotke M, Schreiner PR. *Synthesis* 2007:779–790. This proposal is analogous to the proposed mechanism of 4a-catalyzed imine hydrocyanation (*vide infra*).
48. Larger differences in rate between reactions promoted by 4a and 5 are observed with more electron-deficient substrates (Figures 4 and 5). (The experiments that led to Figures 4 and 5 are run under identical conditions, except that the concentration of 5 is 2.5-fold greater than that of 4a.)
49. Relative rate data were obtained under pseudo first-order conditions at 0 °C. Because enantioselectivity depends on the reaction conditions, intrinsic enantiomeric ratios (*er*) were estimated from experiments run at high dilution ($[\text{imine}]_i = 0.020 \text{ M}$, $-30 \text{ }^\circ\text{C}$). Details are included in the Supporting Information.
50. The relative rate data should be interpreted with caution, as relative rates do not necessarily correlate with the ability of catalysts to stabilize the rate-limiting hydrocyanation transition structures; differences in catalyst aggregation, internal bond rotation, and potential to catalyze hydrocyanation via higher-order mechanisms could each contribute to the relative rate constants. For a discussion on the limitations of using “ k_{rel} ” for the elucidation of complex reaction mechanisms, see: Sun X, Collum DB. *J Am Chem Soc* 2000;122:2452–2458.
51. For an example in the context of organocatalysis in which the free energy and enthalpy of substrate binding to an H-bond donor has been determined, see: ref 45.
52. For a review of the Curtin-Hammett principle, see: Seeman JI. *Chem Rev* 1983;83:83–134.
53. For a well-studied example of a small molecule-catalyzed reaction in which the rate of substrate-catalyst complex formation and dissociation and the rates of reaction are similar, see: Landis CR, Halpern J. *J Am Chem Soc* 1987;109:1746–1754.
54. Bachrach, SM. *Computational Organic Chemistry*. Wiley; Hoboken, NJ: 2007.

55. Allemann C, Gordillo R, Clemente FR, Cheong PHY, Houk KN. *Acc Chem Res* 2004;37:558–569. [PubMed: 15311955]
56. Calculations were executed within Gaussian 03 (Revision E.01), Frisch, MJ., et al. Gaussian, Inc; Wallingford, CT: 2004.
57. For a comparison of these computational methods in the context of asymmetric catalysis, see: Li X, Liu P, Houk KN, Birman VB. *J Am Chem Soc* 2008;130:13836–13837. [PubMed: 18817392]
58. An analogous mechanism that involves proton transfer from the other thiourea *N*-proton has also been characterized by computational methods, and has a slightly higher activation energy.
59. (a) Bordwell FG, Algrim DJ, Harrelson JA Jr. *J Am Chem Soc* 1988;110:5903–5904. (b) Bordwell FG, Ji GZ. *J Am Chem Soc* 1991;113:8398–8401.
60. Expected relative rates of catalysis can be estimated from this energy difference: $\text{rate}_{\text{thiourea}}/\text{rate}_{\text{urea}} \approx e^{(-\Delta\Delta E^\ddagger/RT)} = 20,000$ at 0 °C.
61. Reactions run to greater than one catalytic turnover show substantial amounts of proton exchange both in the presence and absence of substrate, and consequently display significant proton-incorporation into the α -aminonitrile product. Details are provided in the Supporting Information.
62. It is possible, in principle, that the simplified computational model over-estimates the acidity of the thiourea protons or the basicity of the partially-formed α -aminonitrile anion, and that no proton transfer between thiourea and imine occurs. Within this alternative mechanism, the partially formed α -aminonitrile anion would be stabilized by H-bonding in an interaction reminiscent of those interactions present in an enzymatic oxyanion hole (see: ref 16c, and refs therein). This mechanistic proposal is depicted in Scheme 4A, and is inconsistent with the Hammett analysis (Figure 4).
63. One possible mechanism for HCN–HNC isomerization is via a cyclic trimer or higher oligomer: Sánchez M, Provasi PF, Aucar GA, Alkorta I, Elguero J. *J Phys Chem B* 2005;109:18189–18194. [PubMed: 16853336] HCN–HNC isomerization in the presence of imine and catalyst is also possible, and the process may in principle occur on the catalytic cycle (see the Supporting Information).
64. Bürgi HB, Dunitz JD, Shefter E. *J Am Chem Soc* 1973;95:5065–5067.
65. For a discussion of H-bonding, see: Jeffrey, GA. *An Introduction to Hydrogen Bonding*. Oxford University Press; New York: 1997.
66. For a detailed analysis of the relative reactivity of HCN and HNC in catalyst-controlled cyanide addition to aldehydes, and leading references, see: Baeza A, Nájera C, Sansano JM, Saá JM. *Chem Eur J* 2005;11:3849–3862.
67. The calculated activation barrier for the analogous process catalyzed by urea 8b is 1.4 kcal/mol higher than the process catalyzed by thiourea 8a.
68. The conclusions described in this paper for HNC-addition also apply to HCN-addition. All data for the HCN-addition mode are included in the Supporting Information.
69. This simplified model system predicts a small preference for formation of (*S*)- α -aminonitrile, whereas (*R*)- α -aminonitrile is obtained from hydrocyanation reactions using the full catalyst. For consistency, all schemes in this chapter depict formation of (*R*)- α -aminonitrile. The corresponding schemes for formation of (*S*)- α -aminonitrile are included in the Supporting Information.
70. Donoghue PJ, Helquist P, Norrby PO, Wiest O. *J Am Chem Soc* 2009;131:410–411. [PubMed: 19140780]
71. Schneebeli ST, Hall ML, Breslow R, Friesner R. *J Am Chem Soc* 2009;131:3965–3973. [PubMed: 19243187]
72. Streitwieser A Jr, Jagow RH, Fahey RC, Suzuki S. *J Am Chem Soc* 1958;80:2326–2332.
73. E.g., in cyanide addition to aldehydes: Okano V, do Amarol L, Cordes EH. *J Am Chem Soc* 1976;98:4201–4203.
74. (a) Gajewski JJ, Ngermmeesri P. *Org Lett* 2000;2:2813–2815. [PubMed: 10964372] (b) Gajewski JJ, Bocian W, Brichford NL, Henderson JL. *J Org Chem* 2002;67:4236–4240. [PubMed: 12054959]
75. (a) Perrin CL, Ohta BK, Kuperman J. *J Am Chem Soc* 2003;125:15008–15009. [PubMed: 14653734] (b) Perrin CL, Ohta BK, Kuperman J, Liberman J, Erdélyi M. *J Am Chem Soc* 2005;127:9641–9647. [PubMed: 15984892] (c) Perrin CL, Dong Y. *J Am Chem Soc* 2008;130:11143–11148. [PubMed: 18661997]

76. The origins of this effect have been ascribed to a modulation of the C–H stretching frequency. See ref 75b for the determination of this EIE and a discussion of its origins. In that paper, EIEs are expressed in terms of the acidity of the conjugate acid of the amines.
77. Determined at 298.15 K. Explicit solvation by water likely accounts for some of the discrepancy between experiment and computation, as larger β -EIEs were observed in a more limited experimental study in DMSO.
78. Bellamy LJ, Mayo DW. *J Phys Chem* 1976;80:1217–1220.
79. We used this computational method to allow direct comparison with the results in ref 74b.
80. This isotope effect was calculated from the calculated 3N – 6 normal mode vibrational frequencies using the isotopic partition function of Biegeleisen and Mayer at T = 298.15 K. In each case, sufficiently tight geometry optimization convergence criteria were used so that all non-vibrational frequencies (i.e., the six rotational and translational frequencies) were negligible (-1 cm^{-1} to 1 cm^{-1}) compared with the vibrational frequencies ($> 100 \text{ cm}^{-1}$). See: Wolfsberg, M. Comments on Selected Topics in Isotope Theoretical Chemistry. In: Kohen, A.; Limbach, H-H., editors. *Isotope Effects in Chemistry and Biology*. CRC Press; Boca Raton: 2006. Chapter 3
81. This kinetic isotope effect was determined by ^1H -NMR spectroscopy through competition experiments of reactions run to approximately 70% conversion, in which the hydrogen/deuterium ratios were determined in both product and recovered starting material. Details are provided in the Supporting Information.
82. We have also calculated analogous kinetic isotope effects for transition structure D in Scheme 8 relative to free imine at the B3LYP/6-31G(d) level using $3N^{\ddagger} - 7$ vibrational modes for D. The predicted $k_{\text{H}}/k_{\text{D}} = 0.86$ at 298 K or $k_{\text{H}}/k_{\text{D}} = 0.82$ at 243 K is similar to the experimentally observed KIE (eq 5).
83. Several lines of evidence suggest that the pathways leading to (*R*)- and (*S*)-3a are mechanistically consistent for the different catalysts. For example, the same trends in enantioselectivity are observed for both aromatic and aliphatic imines, and under a broad range of different conditions, including different temperatures, cyanide sources, and concentrations. Data are included in the Supporting Information.
84. Statistical analysis was performed using SigmaPlot 10.0 purchased from Systat Software.
85. Alanine-derived catalyst 4h represents the large positive outlier in Figures 11 and 12. This catalyst is also substantially less reactive than any other catalyst, perhaps as a result of catalyst aggregation. It is likely that the experimentally measured enantioselectivity reflects a significant background racemic pathway and therefore underestimates the intrinsic enantioselectivity for this catalyst.
86. B3LYP has been shown to under-estimate the energy of some attractive non-covalent interactions, whereas MP2 over-estimates the energy of these interactions. In this reaction, enantioselectivity is controlled only by non-covalent interactions between substrates and catalysts, and the correlation in Figures 11–12 might be expected to depend strongly of the level of theory used. This is not the case. This conclusion may be ascribed to the observation that the calculated (and experimental; see Figure 4) transition structures are highly charged, and thus the non-covalent interactions responsible for asymmetric induction are expected to have a large electrostatic component. Even ab initio computational methods that do not account for electron correlation (i.e., Hartree-Fock) can account for electrostatic contributions of otherwise complex non-covalent interactions: Mecozzi S, West AP Jr, Dougherty DA. *J Am Chem Soc* 1996;118:2307–2308.
87. Calculated versus experimental selectivity plots for HCN-addition are included in the Supporting Information. Statistically significant positive linear correlation is observed in all cases. HCN-addition is disfavored compared with HNC addition for each catalyst at each level of theory examined (by 0.2–3.7 kcal/mol). The transition structures for HNC addition and HCN addition are similar, and the ion pairs formed from HNC-addition and HCN-addition are almost identical; it is thus not possible to further distinguish between these two mechanistic proposals, and it is possible that both play a role in catalytic imine hydrocyanation.
88. The length of the *N*–H bond between imine and proton is 1.03–1.04 Å in the transition structure, and is thus effectively fully formed (i.e., the transition structure has nearly complete iminium ion character).
89. This analysis ignores any role of bond angle in determining bond energy, and ignores the possibility that bond strength does not necessarily depend linearly on bond length.

90. See, for example: (a) ref 44. Mita, T.; Jacobsen, EN. *Synlett*. 2009. p. 1680-1684.
91. For examples of cationic chiral catalysts thought to operate through non-covalent interactions see: (a) Hashimoto T, Maruoka K. *Chem Rev* 2007;107:5656–5682. [PubMed: 18072806] (b) Uyeda C, Jacobsen EN. *J Am Chem Soc* 2008;130:9228–9229. [PubMed: 18576616] For computational analysis of reactions catalyzed by chiral, quaternary ammonium salts (i.e., phase-transfer catalysis), see: (c) Cannizarro CE, Houk KN. *J Am Chem Soc* 2002;124:7163–7169. [PubMed: 12059242] (d) Gomez-Bengoa E, Linden A, López R, Múgica-Mendiola I, Oiarbide M, Palomo C. *J Am Chem Soc* 2008;130:7955–7966. [PubMed: 18510320] See, also: (e) Corey EJ, Xu F, Noe MC. *J Am Chem Soc* 1997;119:12414–12415.
92. For examples of anionic chiral catalysts thought to operate through non-covalent interactions, see: (a) Mayer S, List B. *Angew Chem, Int Ed* 2006;45:4193–4195. (b) Hamilton GL, Kanai T, Toste FD. *J Am Chem Soc* 2008;130:14984–14986. [PubMed: 18937464] For a review on chiral anions, see: (c) Lacour J, Hebbe-Viton V. *Chem Soc Rev* 2003;32:373–382. [PubMed: 14671792]
93. For other examples of neutral chiral catalysts thought to operate through non-covalent interactions, see: ref 1.
94. See, for example: (a) ref 20, Chapter 2 (covalent catalysis), Chapter 3 (general acid-base catalysis), and Chapters 6 and 7 (hydrogen bonding and electrostatic forces in catalysis). Silverman, RB. *The Organic Chemistry of Enzyme-Catalyzed Reactions*. Academic Press; San Diego: 2002. p. 18-20. (covalent catalysis), pp 20–28 (general acid-base catalysis), pp 28–30 (electrostatic catalysis)
95. Segel, IH. *Enzyme Kinetics*. John Wiley & Sons; New York: 1975.
96. See, for example, the discussions in: (a) Lipscomb WN. *Acc Chem Res* 1982;15:232–238. (b) Benkovic SJ, Hammes-Schiffer S. *Science* 2003;301:1196–1202. [PubMed: 12947189]
97. The imine binding constant in the kinetic analysis of reactions catalyzed 1b is small ($K_M = 0.214 \pm 0.009$ M). Under the conditions of our kinetic analysis with catalyst 4a, we estimate that K_M values less than 0.5 would be detectable. The differences in binding constant observed in the two analyses may be ascribed to differences in reaction temperature (–78 °C versus 0 °C) and/or to the imine *N*-protecting group (allyl versus benzhydryl).
98. Even in cases in which electrophile–thiourea interactions are productive, the binding geometry in the ground state can differ substantially from that in the transition state. For example, ketone–thiourea binding can occur through one or both lone pairs of the carbonyl group, and the calculated energies of these binding modes are nearly identical (Fuerst, D.E. Unpublished results from this laboratory). In the nucleophilic addition transition structure, the partially formed alkoxide binds in a way that resembles neither of the low-energy ground state structures (ref 16c).
99. For a related analysis comparing binding geometries of carbonyl compounds to chiral diols in the ground state and transition state, see: Gómez-Bengoa E. *Eur J Org Chem* 2009:1207–1213.
100. For an alternative approach, see: (a) Pluth MD, Bergman RG, Raymond KN. *Science* 2007;316:85–88. [PubMed: 17412953] (b) Pluth MD, Bergman RG, Raymond KN. *J Org Chem* 2009;74:58–63. [PubMed: 19113901] and refs therein

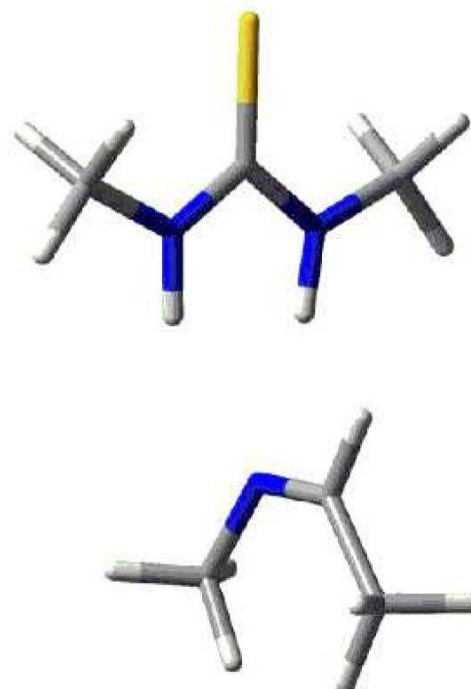
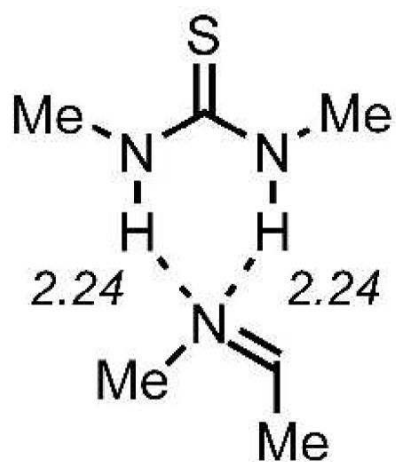


Figure 1. Dual H-bonding interaction between imine and thiourea. The three-dimensional structure is a local minimum at the B3LYP/6-31G(d,p) level of theory.

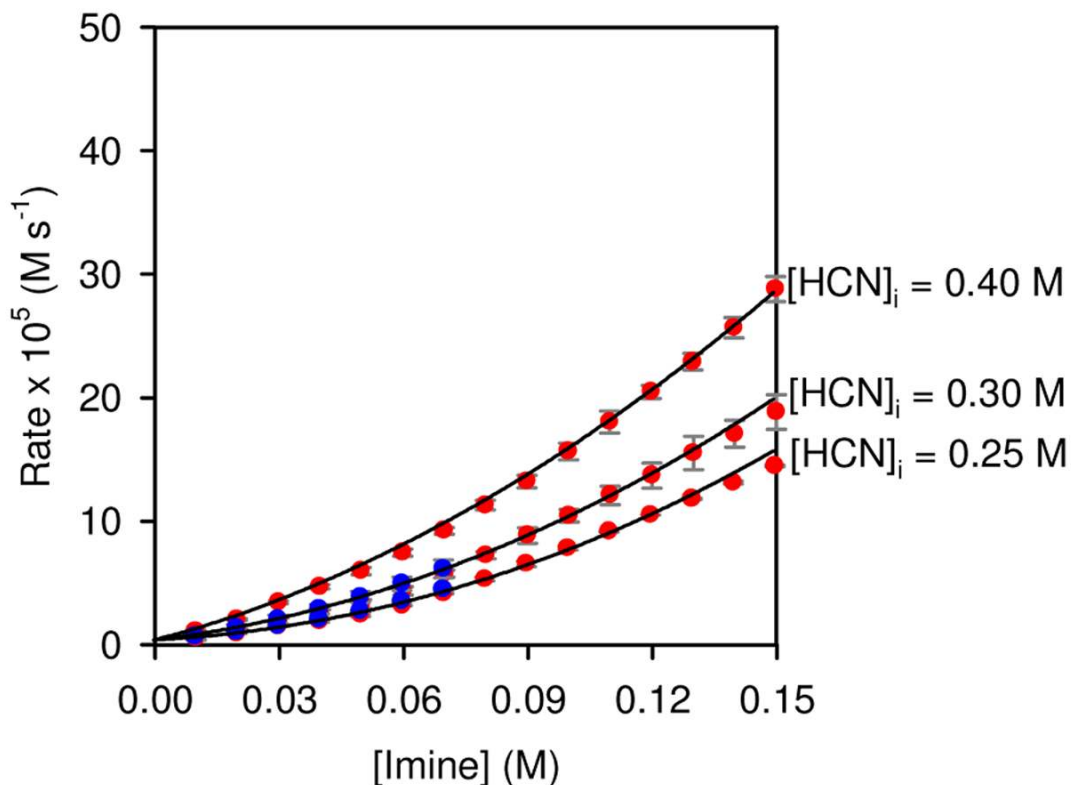


Figure 2.

Rate dependence on [HCN] and [imine]. Plot of rate of imine hydrocyanation catalyzed by **4a** ($[\text{cat}]_{\text{tot}} = 0.0040 \text{ M}$) versus [imine] at different $[\text{HCN}]_i$. Each set of points represents the average rate determined from two individual kinetics experiments with $[\text{imine}]_i = 0.20 \text{ M}$ (red points) or $[\text{imine}]_i = 0.10 \text{ M}$ (blue points). The black curves represent least-squares fits of the experimental rate versus conversion data to eq 1.

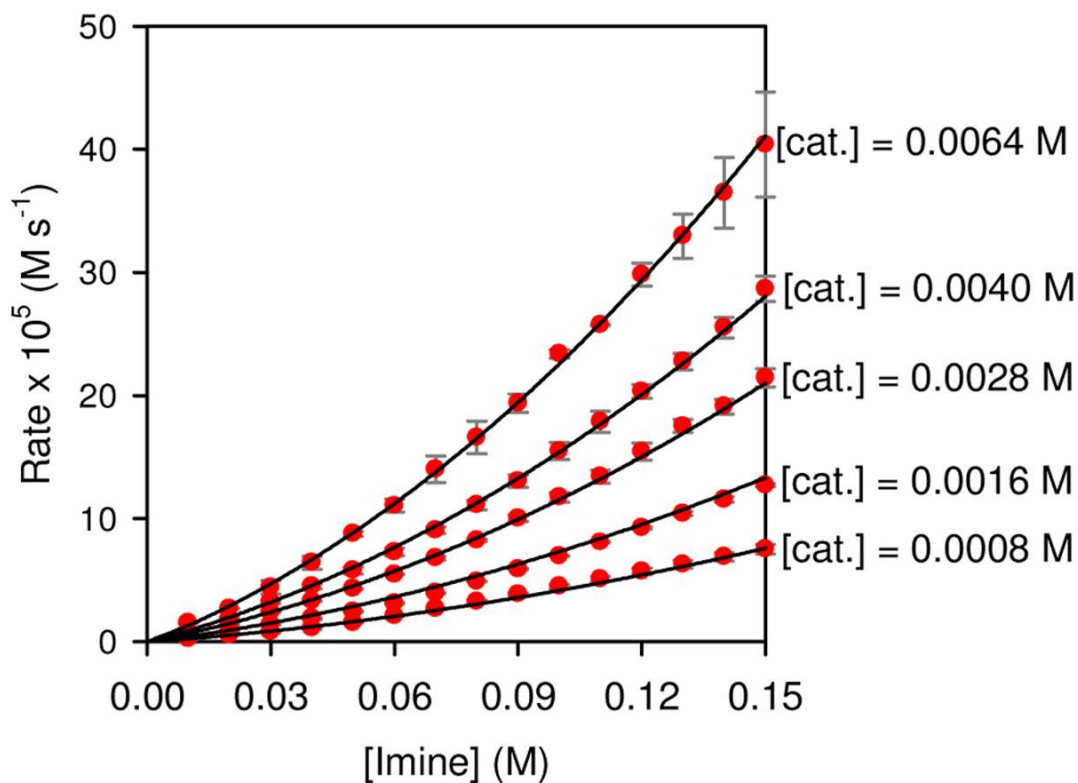


Figure 3. Rate dependence on $[\text{cat}]_{\text{tot}}$ and $[\text{imine}]$. Plot of rate of imine hydrocyanation ($[\text{HCN}]_i = 0.25 \text{ M}$) catalyzed by **4a** versus $[\text{imine}]$ at different $[\text{cat}]_{\text{tot}}$. Each set of points represents the average rate determined from two individual kinetics experiments with $[\text{imine}]_i = 0.20 \text{ M}$. The black curves represent least-squares fits of the experimental rate versus concentration data to eq 1.

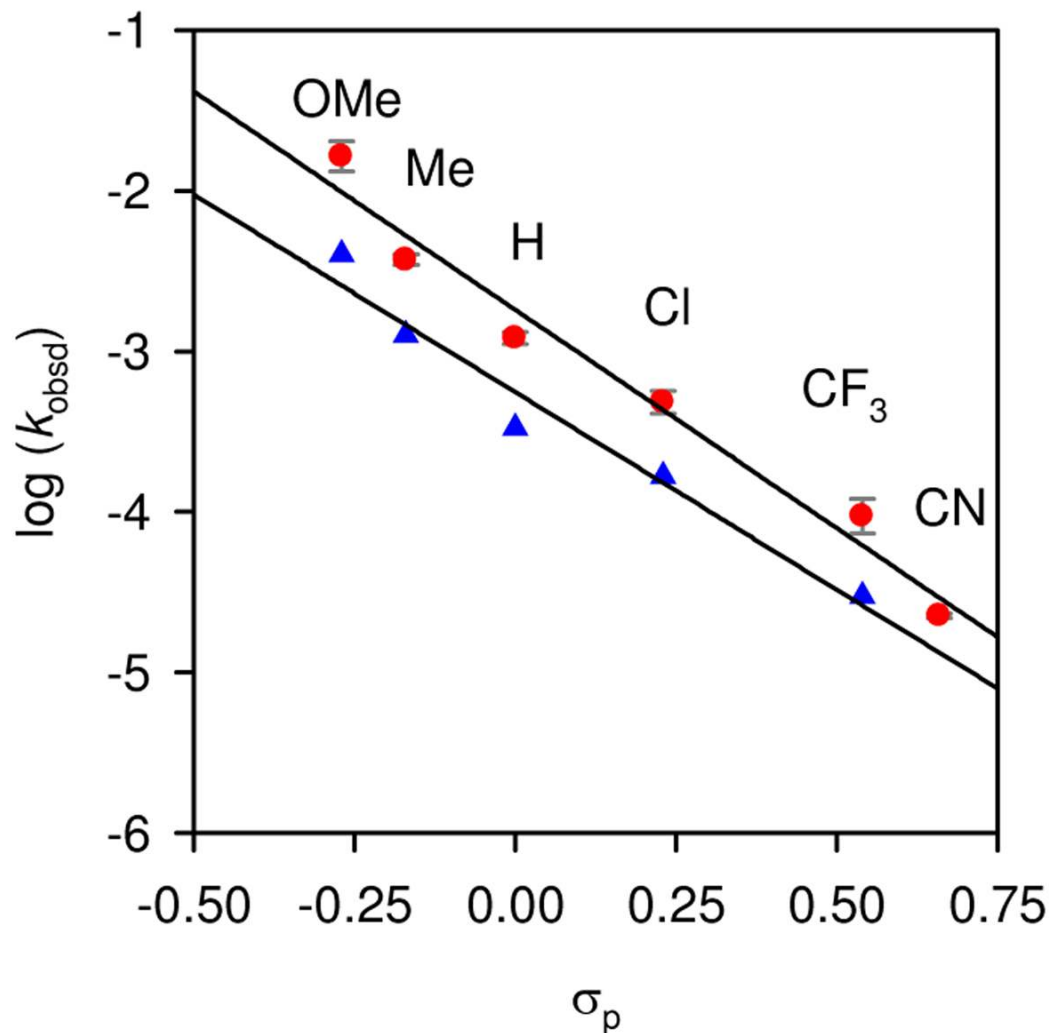


Figure 4. Rate dependence of imine hydrocyanation catalyzed by **4a** or **4b** on substrate electronic properties. Plot of the logarithm of pseudo-first-order rate constant ($\log(k_{\text{obsd}})$) versus σ_p for the hydrocyanation of p-substituted imines **2b–2g** ($[2]_i = 0.040$ M) by TMSCN/MeOH (0.50 M) mediated by thiourea catalyst **4a** ($[\text{cat}]_{\text{tot}} = 0.0020$ M, ■) or urea catalyst **4b** ($[\text{cat}]_{\text{tot}} = 0.0020$ M, ▲) versus σ_p . The black curves represent least-squares fits to $f(x) = a + \rho x$, $a_{\text{thiourea}} = -2.74 \pm 0.06$, $\rho_{\text{thiourea}} = -2.7 \pm 0.2$; $a_{\text{urea}} = -3.25 \pm 0.08$, $\rho_{\text{urea}} = -2.5 \pm 0.2$.

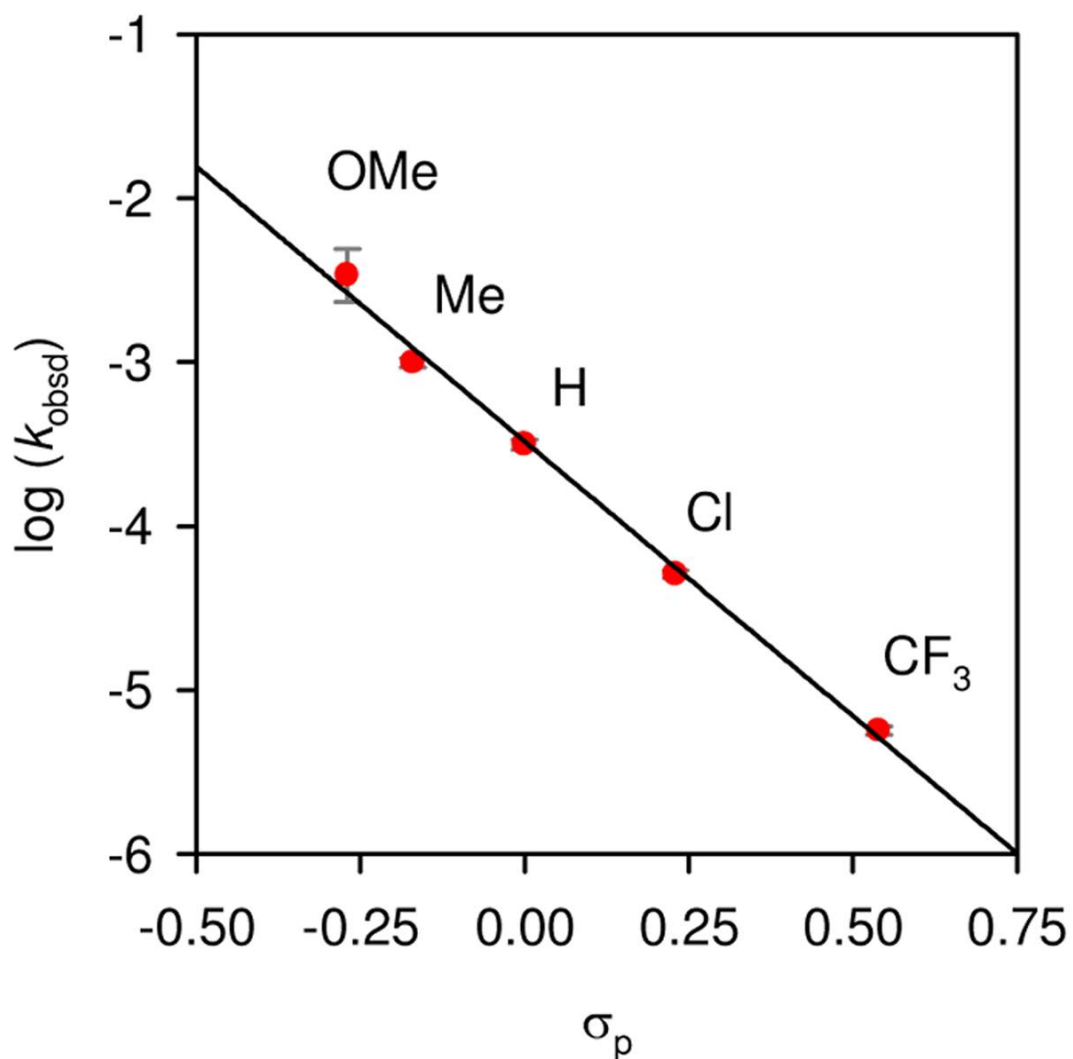


Figure 5. Rate dependence of imine hydrocyanation on substrate electronic properties. Logarithm of pseudo-first order rate constant ($\log(k_{\text{obsd}})$) versus σ_p of the hydrocyanation of *p*-substituted imines **2g–2l** ($[2]_i = 0.040$ M) mediated by TMSCN/MeOH (0.50 M) and thiourea catalyst **5** (0.0050 M). The black curve depicts an unweighted least-squares fit to $f(x) = a + \rho x$ ($\rho = -3.3 \pm 0.1$). The experiments leading to Figures 4 and 5 were executed under identical conditions, except that the concentration of **5** was 2.5-fold greater than of **4a** or **4b**.

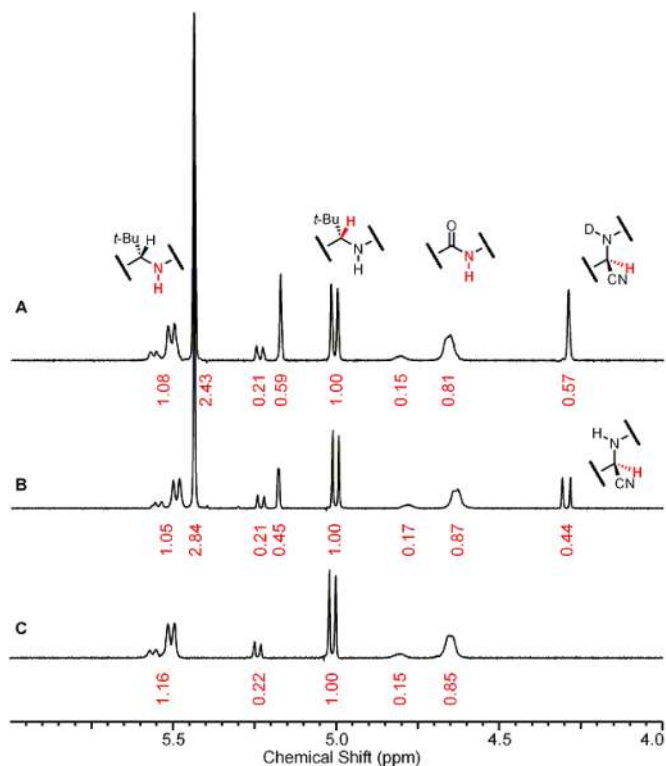


Figure 6. Partial ^1H -NMR spectra of reactions depicted in eq 3 after 25 min using (A) DCN, catalyst **6b**, and imine **2h**, (B) HCN, catalyst **6b**, and imine **2h**, or (C) DCN and catalyst **6b**. Data were collected at 32 °C. Under these conditions, the catalyst exists as a 5:1 mixture of amide rotamers. Deuterium incorporation at the *N*-H position of the α -aminonitrile can be assessed by analyzing the coupling pattern of the C(CN)H proton (δ 4.3 ppm). The experiment containing DCN displays quantitative deuterium incorporation into the α -aminonitrile, whereas the experiment containing HCN displays quantitative proton incorporation into the α -aminonitrile. HCN and DCN were generated from TMSCN and MeOH or MeOD. The enantiomeric excess of the α -aminonitrile isolated from these reactions is 84–85%.

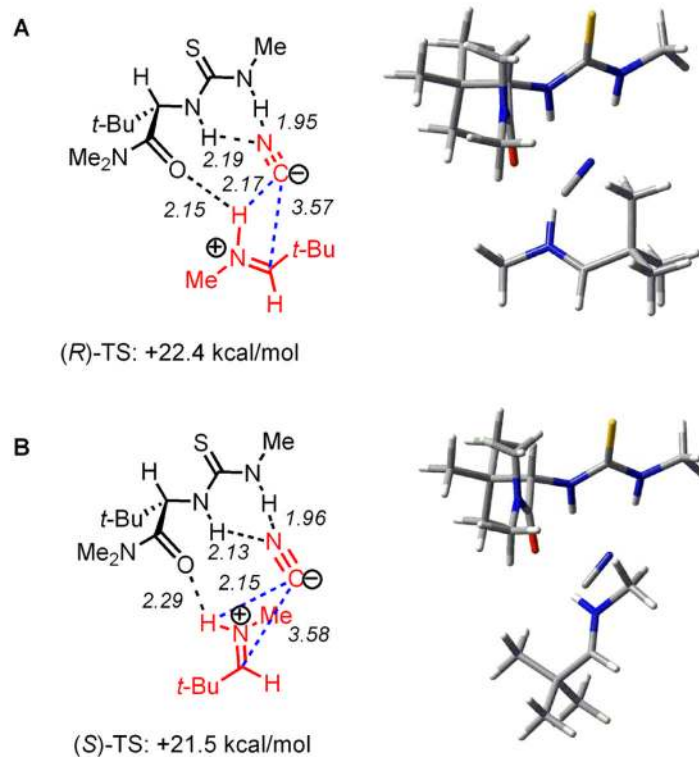


Figure 7. Calculated transition structures for HCN-addition to imine **9a** catalyzed by **8a** (B3LYP/6-31G (d)). Transition structures leading to (A) (*R*)- α -aminonitrile and (B) (*S*)- α -aminonitrile are shown.

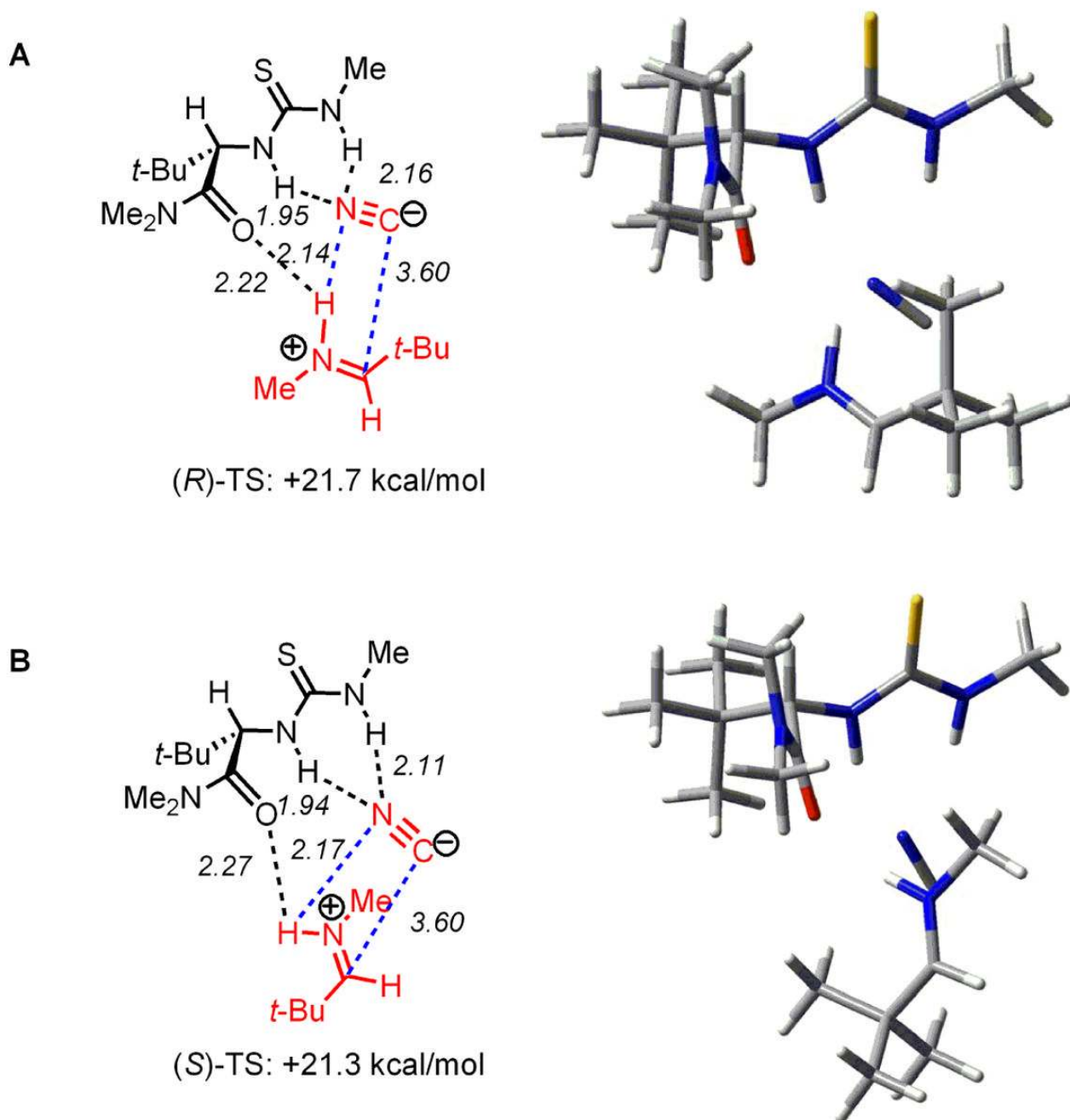


Figure 8. Calculated transition structures for HNC-addition to imine **9a** catalyzed by **8a** (B3LYP/6-31G (d)). Transition structures leading to (A) (*R*)- α -aminonitrile and (B) (*S*)- α -aminonitrile are shown.

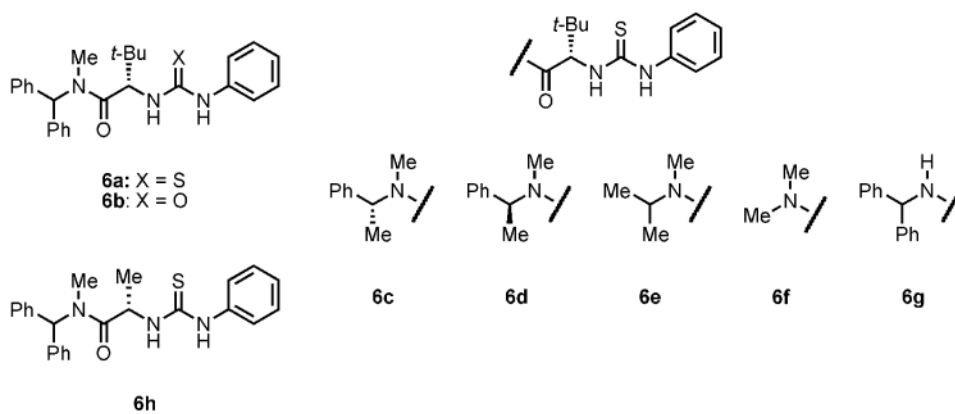


Figure 9.
Amido-thioureas used in quantitative computational analysis.

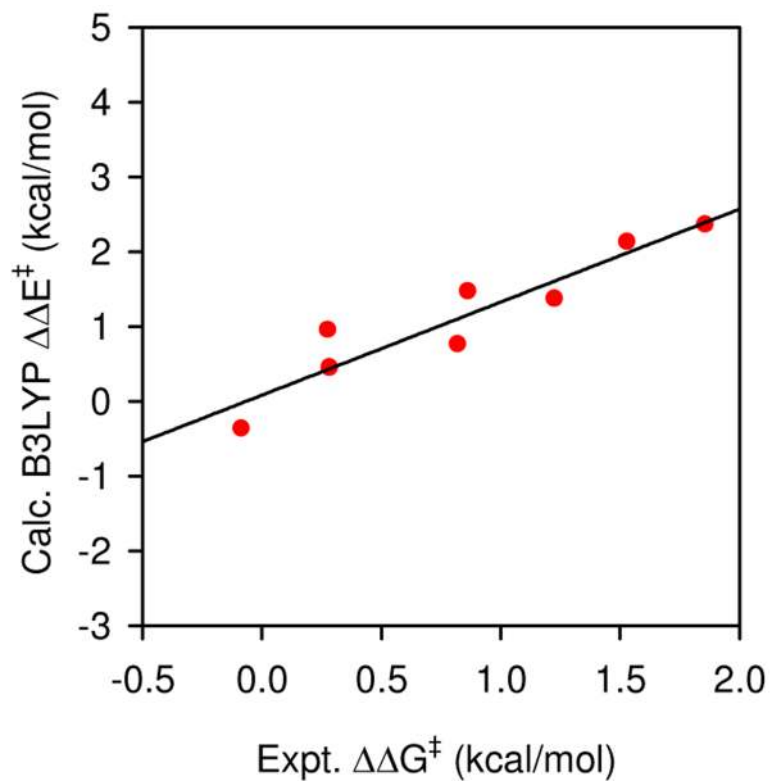


Figure 10. Calculated versus experimental enantioselectivity of HNC addition to **2a** at the B3LYP/6-31G (d) level. Plot of calculated $\Delta\Delta E^\ddagger$ of HNC-addition transition structures versus estimated experimental $\Delta\Delta G^\ddagger$ (Table 2, entries 1, 4–10). The curve represents a least-squares fit to $f(x) = a + bx$, $a = 0.1 \pm 0.2$ kcal/mol, $b = 1.2 \pm 0.2$, $R^2 = 0.87$, $P_b = 0.0006$.

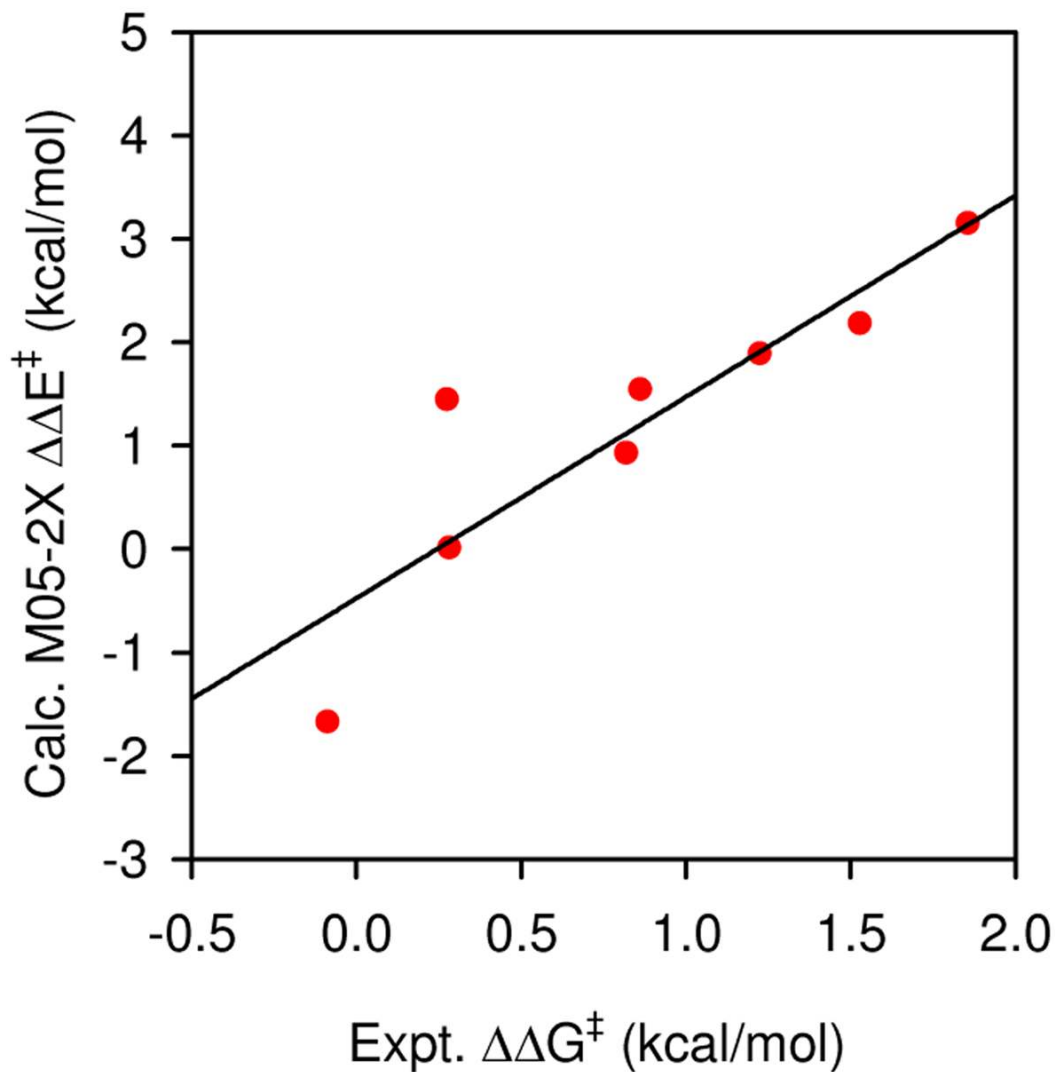


Figure 11.

Calculated versus experimental enantioselectivity of HNC addition to **2a** at the M05-2X/6-31+G(d,p)//B3LYP/6-31G(d) level. Plot of calculated $\Delta\Delta E^\ddagger$ of HNC-addition transition structures versus estimated experimental $\Delta\Delta G^\ddagger$ (Table 2, entries 1, 4–10). The curve represents a least-squares fit to $f(x) = a + bx$, $a = -0.5 \pm 0.4$ kcal/mol, $b = 1.9 \pm 0.4$, $R^2 = 0.79$, $P_b = 0.0033$.

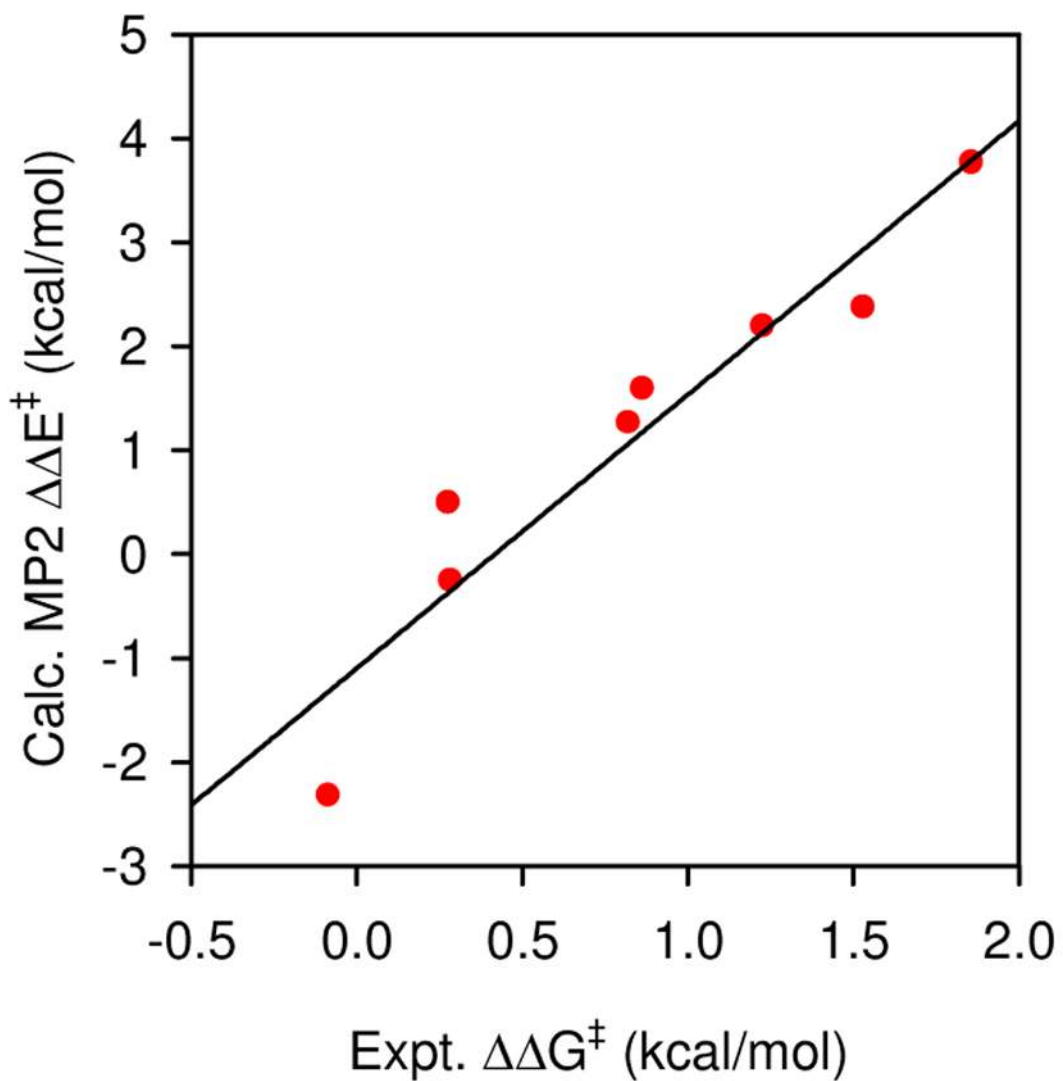


Figure 12.

Calculated versus experimental enantioselectivity of HNC addition to **2a** at the MP2/6-31G(d)//B3LYP/6-31G(d) level. Plot of calculated $\Delta\Delta E^\ddagger$ of HNC-addition transition structures versus estimated experimental $\Delta\Delta G^\ddagger$ (Table 2, entries 1, 4–10). The curve represents a least-squares fit to $f(x) = a + bx$, $a = -1.1 \pm 0.4$ kcal/mol, $b = 2.6 \pm 0.4$, $R^2 = 0.91$, $P_b = 0.0003$.

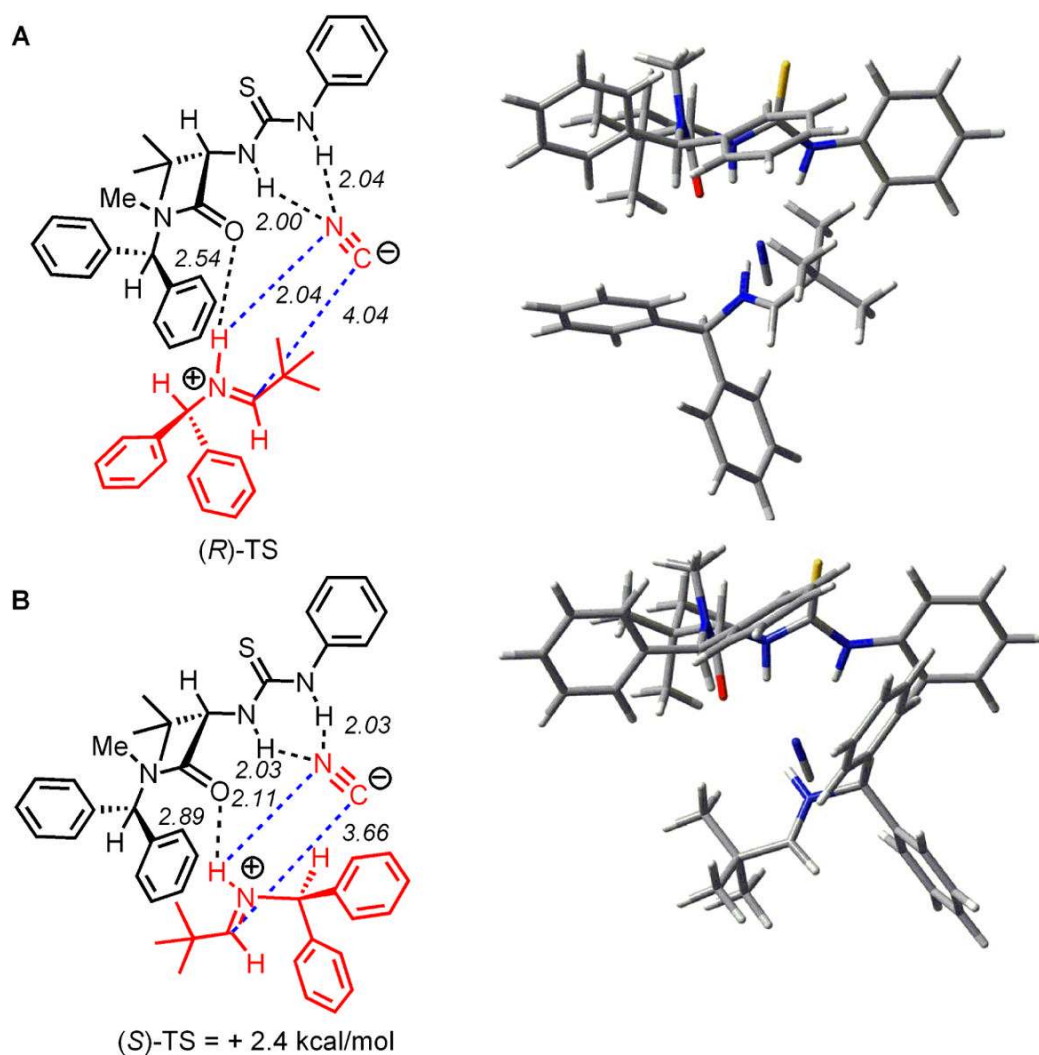


Figure 13. Calculated transition structures for HNC addition to imine **2a** catalyzed by **6a**. Transition structures leading to the (A) major and (B) minor enantiomer are shown.

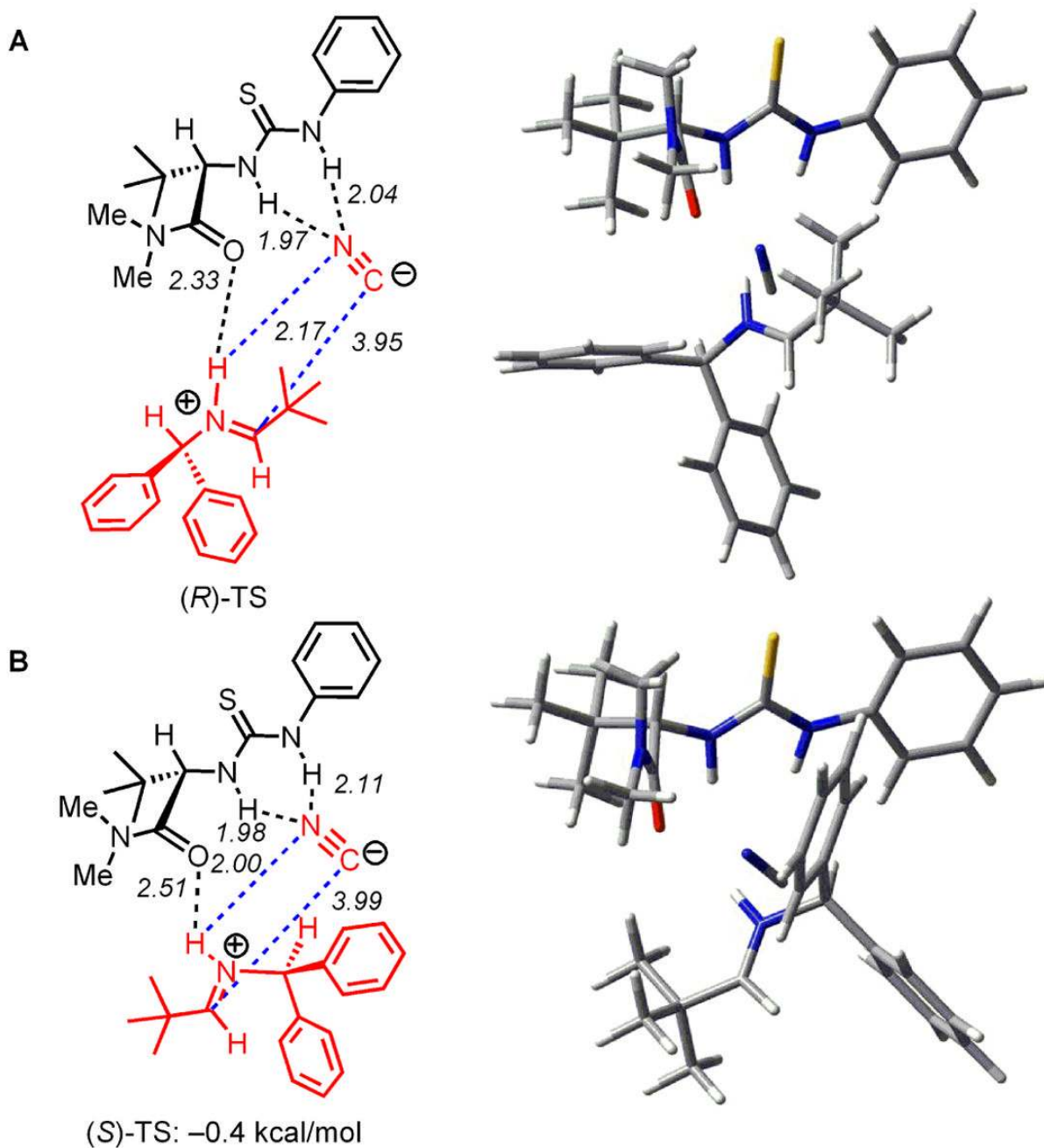


Figure 14. Calculated transition structures for HNC-addition to imine **2a** catalyzed by **6f**. Transition structures leading to the (A) minor and (B) major enantiomer are shown.

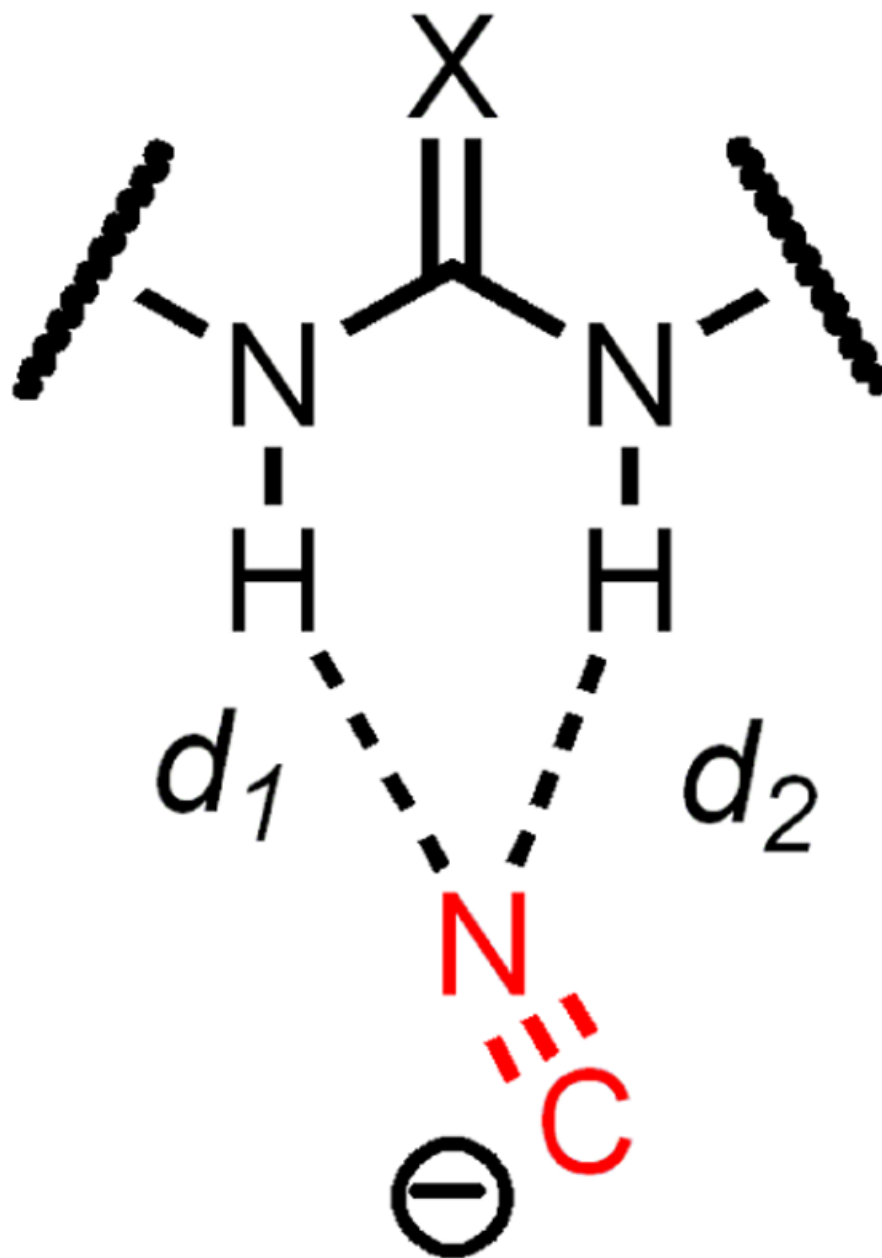


Figure 15.
H-bond distances between thiourea ($X = S$) or urea ($X = O$) and cyanide anion.

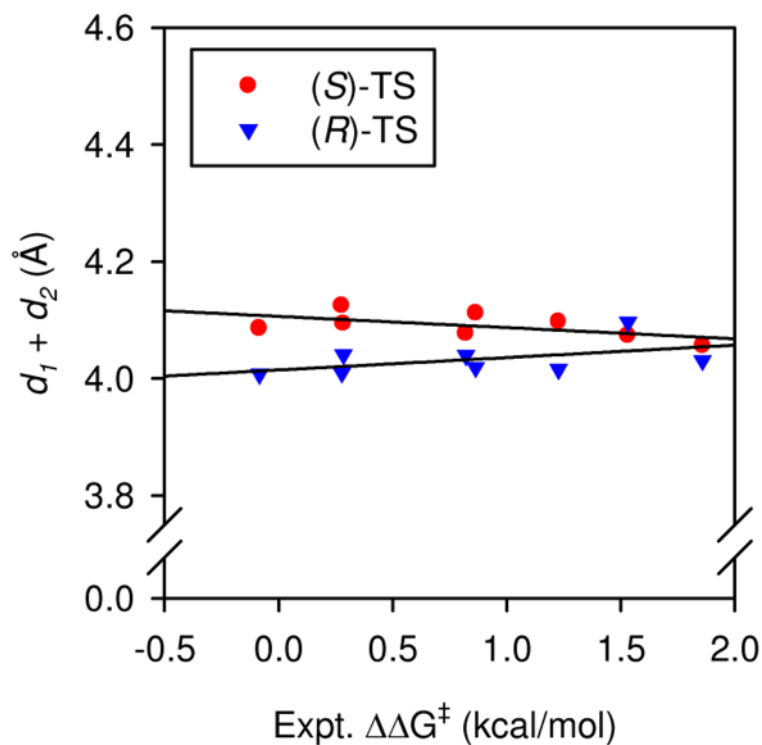


Figure 16. Correlation of transition structure bond length with enantioselectivity for HNC addition to imine **2a**. Plot of the sum of the cyanide–(thio)urea H-bond lengths in B3LYP/6-31G(d) transition structures using catalysts **6a–6h** versus experimental energy difference between (*R*)- and (*S*)-transition states estimated using catalysts **4a–4h** (Table 2). The black curves represent a least-squares fit to $f(x) = a + b x$; (*R*)-TS: $a = 4.01 \pm 0.02 \text{ \AA}$, $b = 0.02 \pm 0.02 \text{ \AA mol kcal}^{-1}$, $R^2 = 0.24$, $P_b = 0.22$; (*S*)-TS: $a = 4.11 \pm 0.01 \text{ \AA}$, $b = -0.01 \text{ \AA mol kcal}^{-1}$, $R^2 = 0.34$, $P_b = 0.13$.

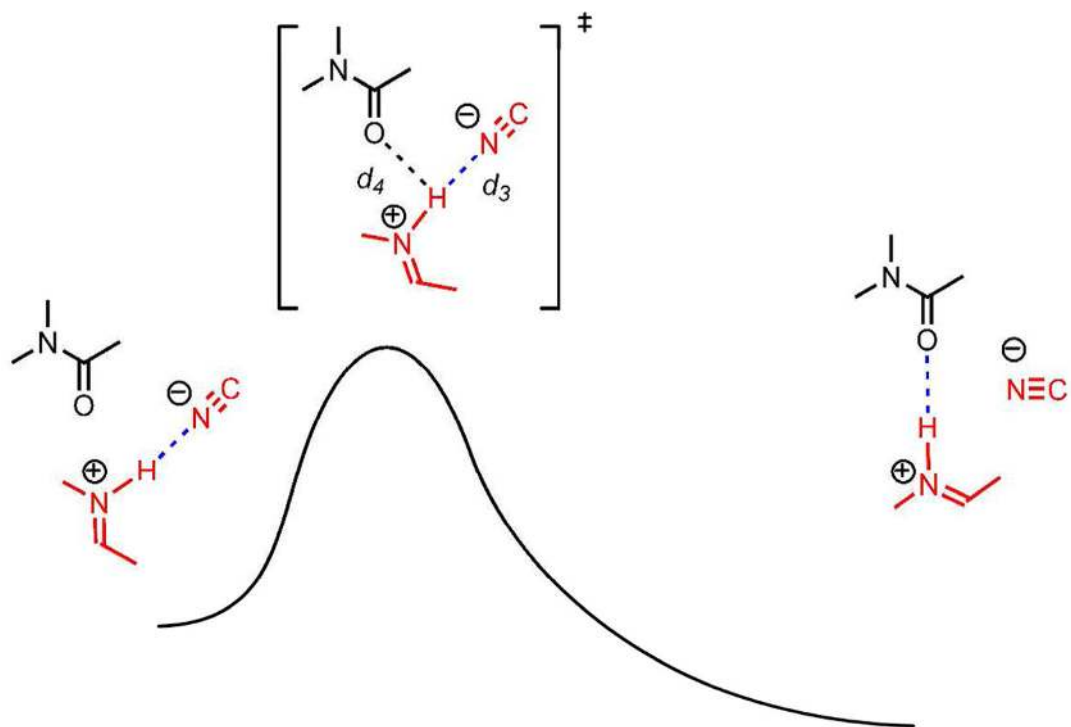


Figure 17. Qualitative reaction coordinate diagram for iminium/cyanide ion pair rearrangement depicting H-bond distances between iminium ion, cyanide anion, and catalyst amide.

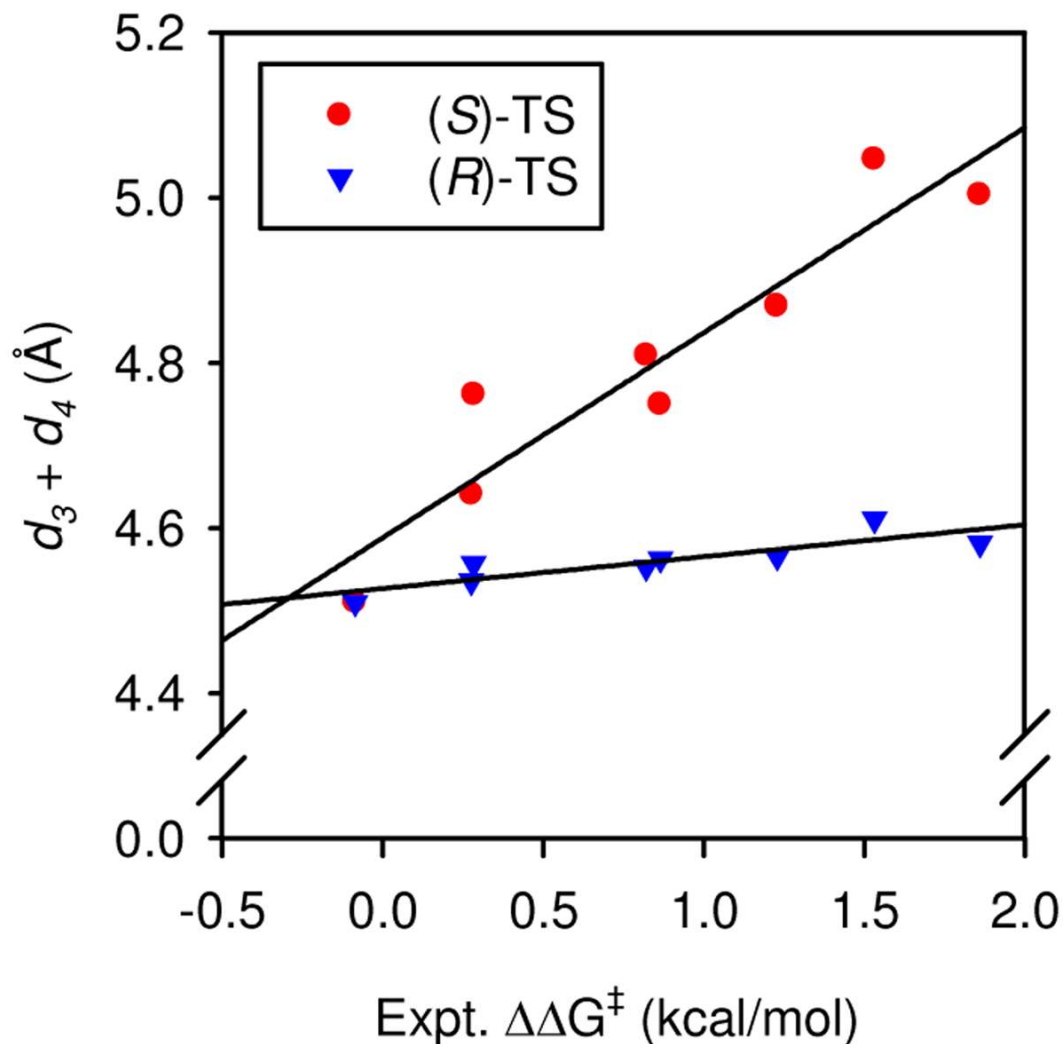
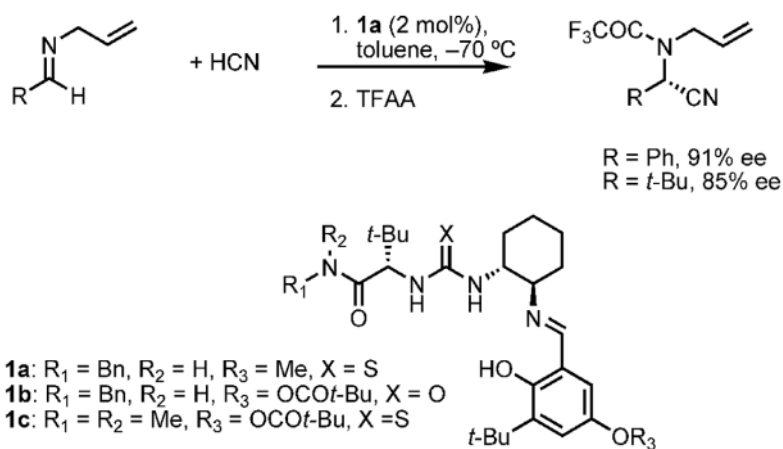
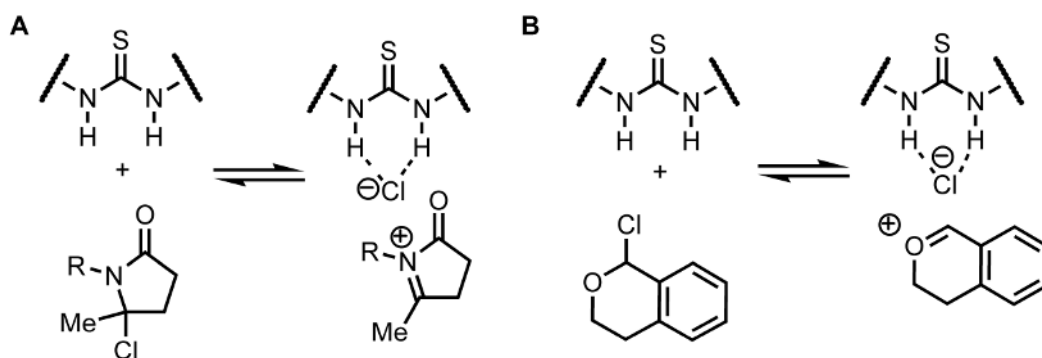


Figure 18.

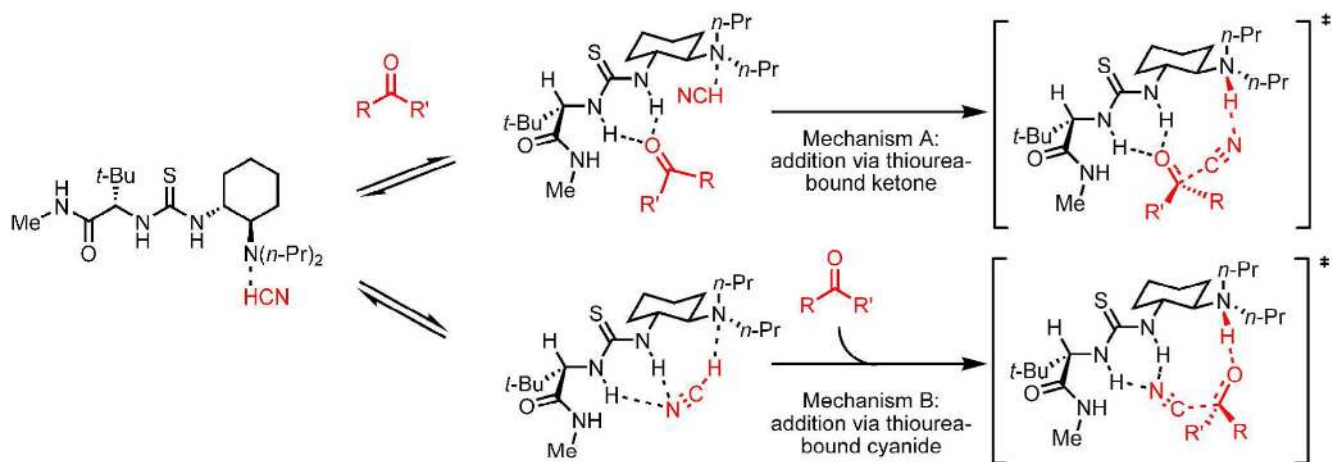
Correlation of transition structure bond length with enantioselectivity for HNC addition to imine **2a**. Plot of the sum of the cyanide N–iminium H + amide O–iminium H bond lengths in B3LYP/6-31G(d) transition structures using catalysts **6a–6h** versus experimental energy difference between (*R*)- and (*S*)-transition structures using catalysts **4a–4h** (Table 2.2). The black curves represent a least-squares fit to $f(x) = a + b x$; (*R*)-TS: $a = 4.527 \pm 0.01$ Å, $b = 0.039 \pm 0.009$ Å mol kcal⁻¹, $R^2 = 0.75$, $P_b = 0.0054$; (*S*)-TS: $a = 4.59 \pm 0.04$ Å, $b = 0.25 \pm 0.04$ Å mol kcal⁻¹, $R^2 = 0.88$, $P_b = 0.0005$.



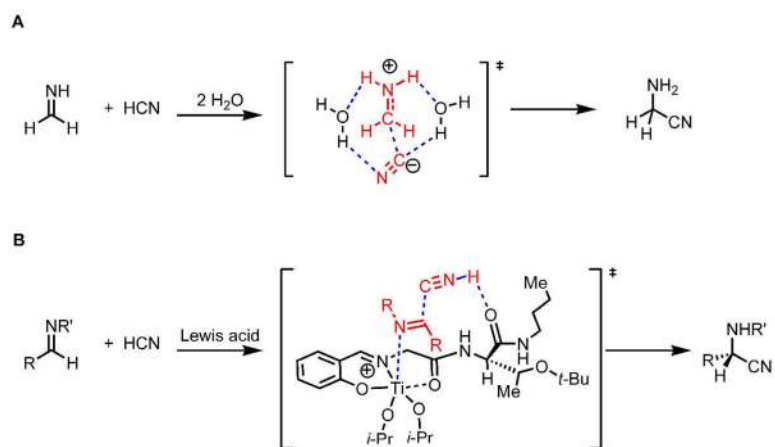
Scheme 1.
Enantioselective imine hydrocyanation catalyzed by chiral (thio)urea derivatives

**Scheme 2.**

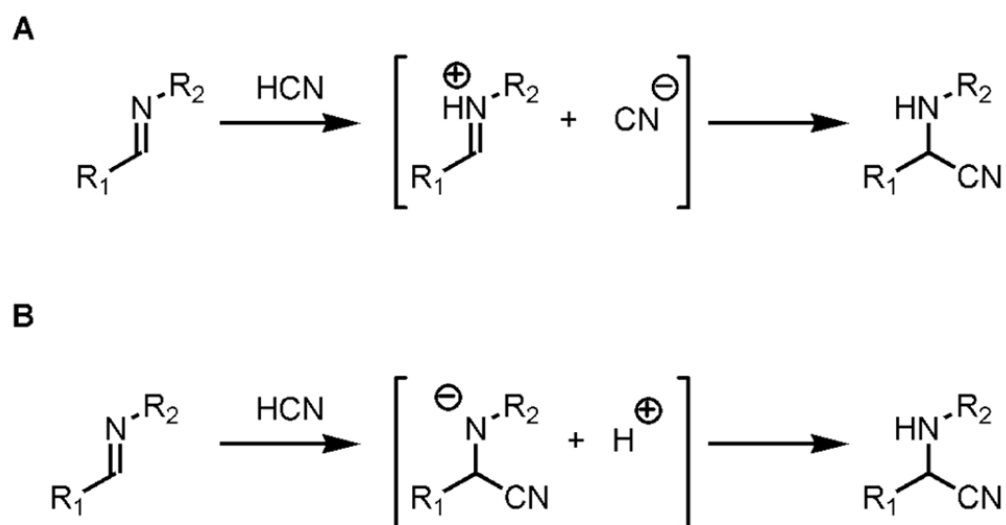
Examples of proposed anion-binding mechanisms promoted by chiral (thio)urea derivatives involving (A) *N*-acyl iminium/chloride and (B) oxocarbenium/chloride ion pairs

**Scheme 3.**

Competing enantioselectivity-determining pathways in the amino-thiourea catalyzed cyanosilylation of ketones (ref ^{16c}). Mechanism A is favored, but both pathways are energetically accessible.

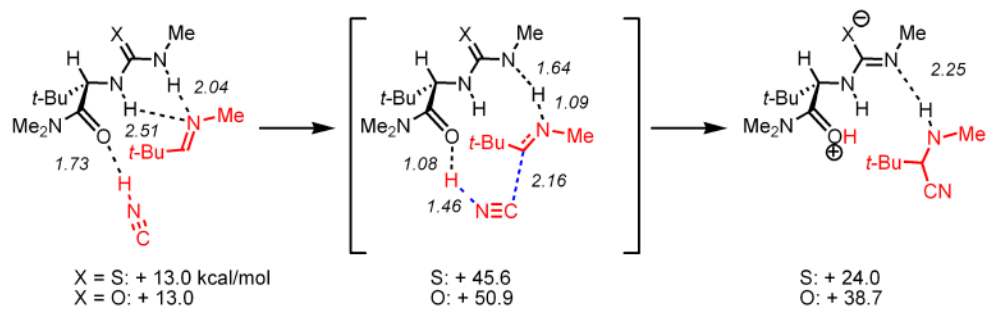


Scheme 4. Proposed transition structures for (A) water-mediated^a and (B) chiral Lewis-acid catalyzed^b imine hydrocyanation
a. ref ²². b. ref ^{25b}



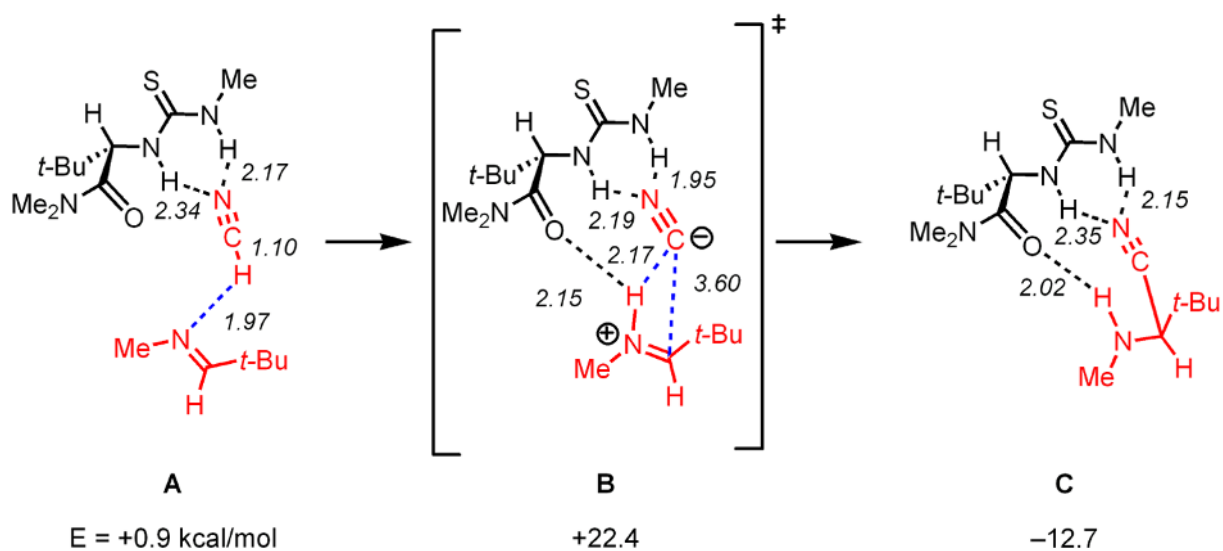
Scheme 5.

Limiting mechanisms for imine hydrocyanation proceeding through (A) an iminium ion or (B) an α-amidocarbonitrile anion.

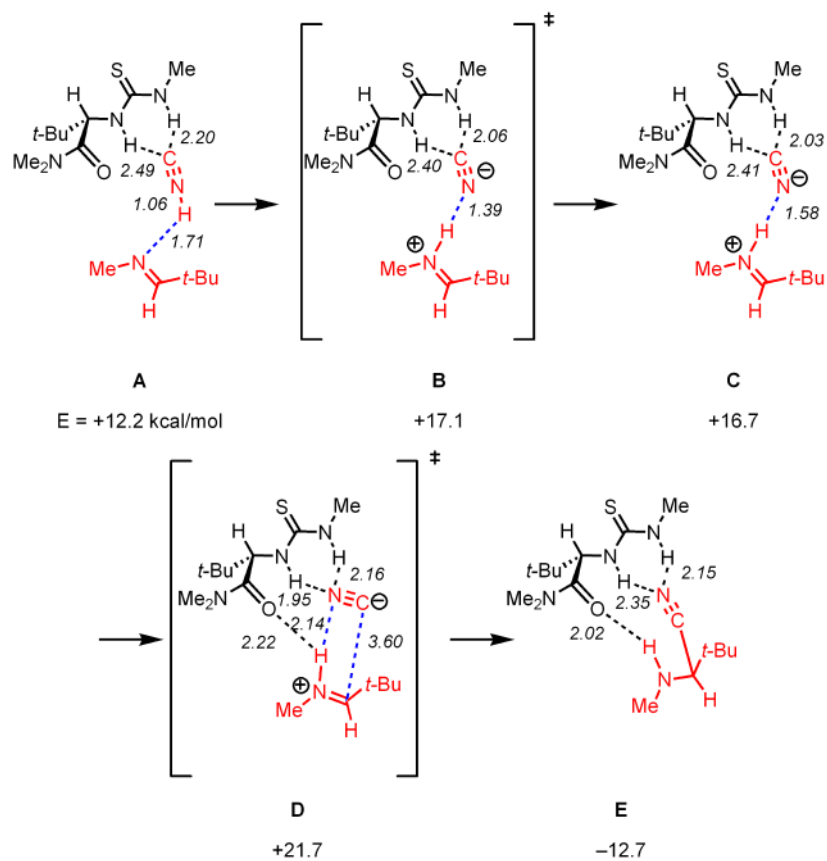


Scheme 6. Amido-(thio)urea controlled HNC addition to imine^a

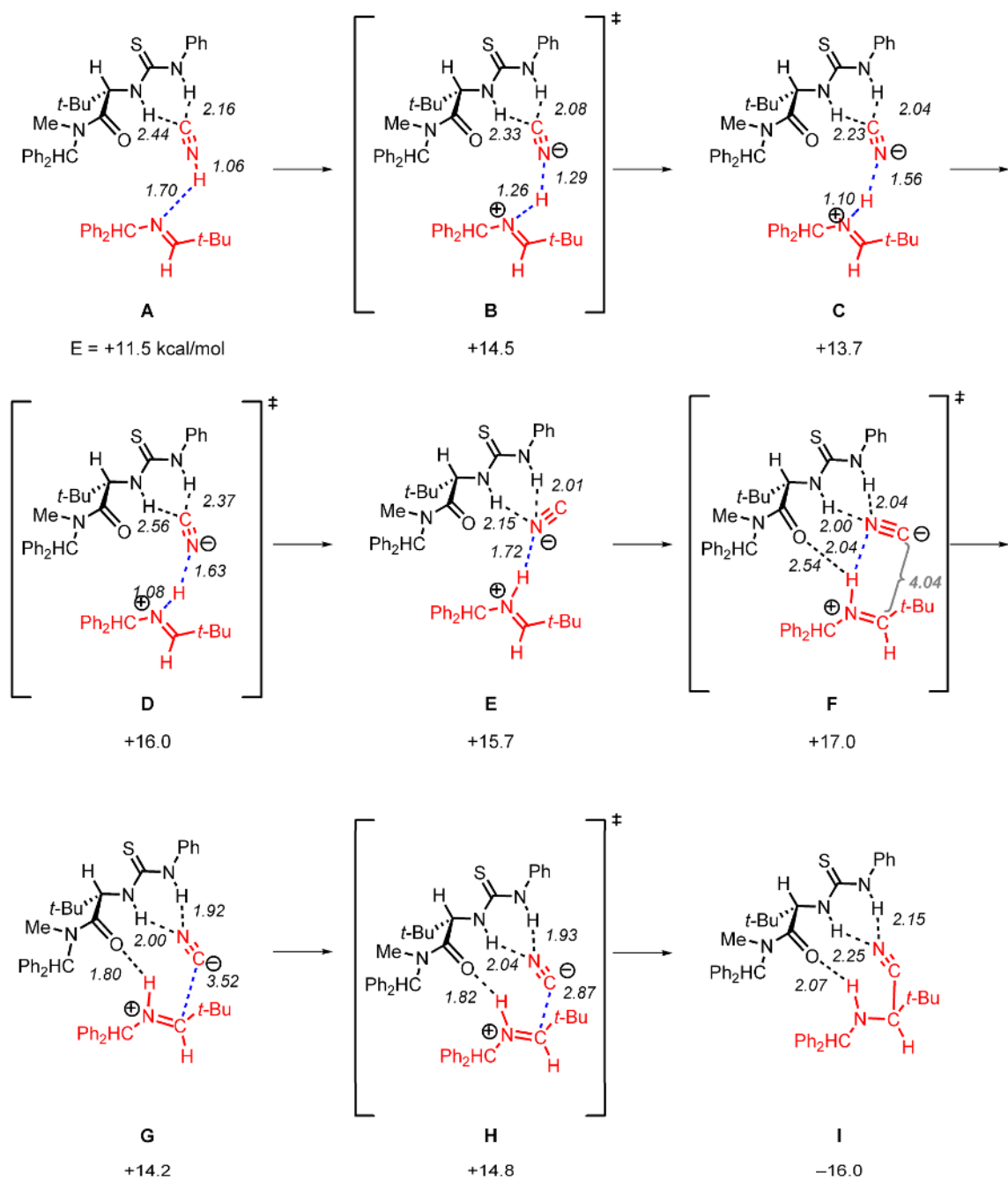
a. Bond distances (Å) for X = S are shown. All energies are relative to the energy calculated for **10a** or the analogous urea-derived complex.



Scheme 7.
Catalyst-controlled, HCN-mediated imine hydrocyanation.



Scheme 8.
Catalyst-controlled, HNC-mediated imine hydrocyanation.



Scheme 9.
Catalyst-controlled, HNC-mediated imine hydrocyanation

Table 1

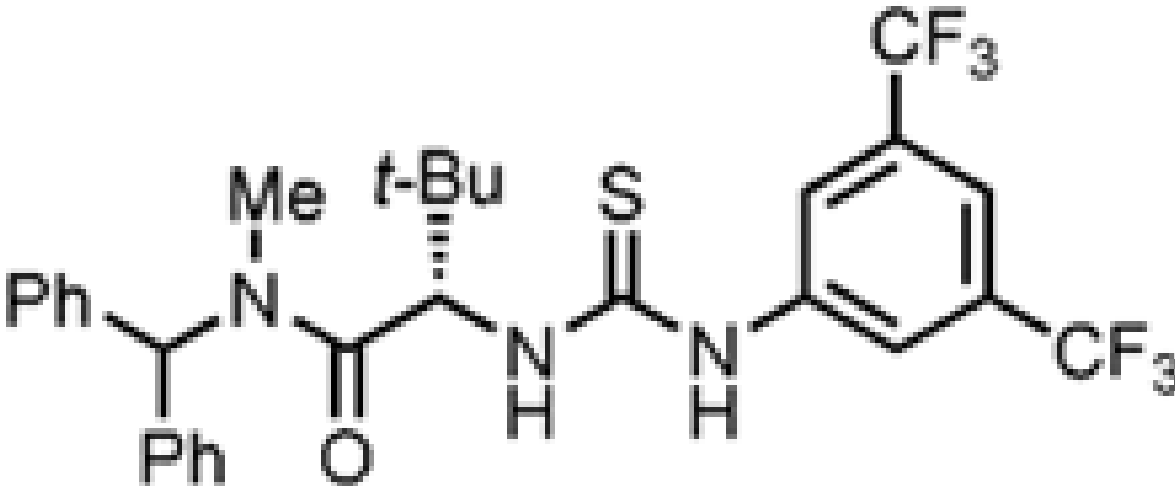
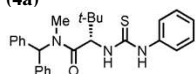
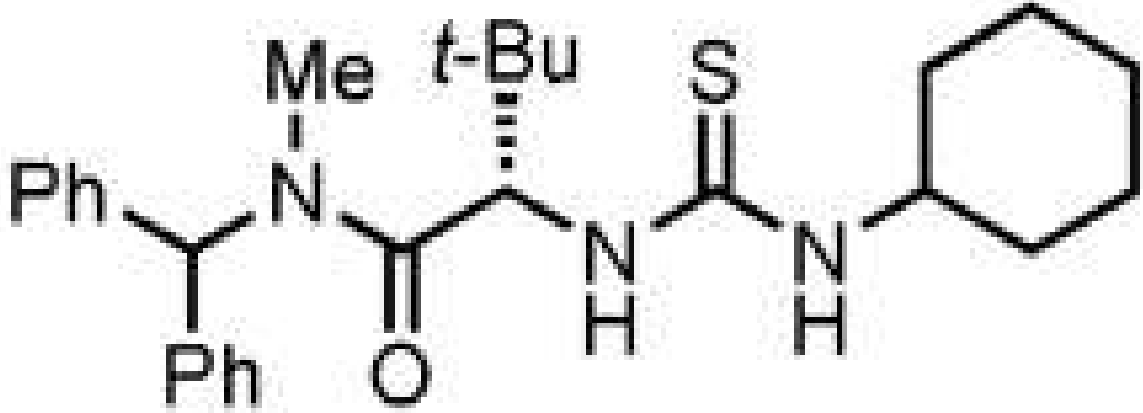
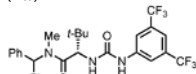
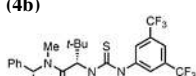
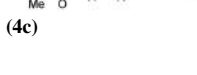
Asymmetric imine hydrocyanation using catalysts **4a** and **4b**.

Entry	cat.	Imine 2 (R =)	cat. (mol%)	Yield ^d (%)	ee ^b (%)
1	4a	<i>tert</i> -butyl (a)	2	99	93
2	4a	<i>p</i> -OMeC ₆ H ₄ (b)	2	99	99
3	4a	<i>p</i> -MeC ₆ H ₄ (c)	2	98	98
4	4a	C ₆ H ₅ (d)	2	98	98
5	4a	<i>p</i> -ClC ₆ H ₄ (e)	2	97	98
6	4a	<i>p</i> -CF ₃ C ₆ H ₄ (f)	2	98 ^c	96
7	4a	<i>p</i> -CNC ₆ H ₄ (g)	10	96 ^c	93
8	4b	<i>p</i> -OMeC ₆ H ₄ (h)	2	98	96
9	4b	C ₆ H ₅ (d)	2	97	93
10	4b	<i>p</i> -CF ₃ C ₆ H ₄ (f)	2	96 ^c	92

^a Isolated yields of **3** after silica gel chromatography of reactions run on 1.0 mmol scale.^b Enantiomeric excess of purified samples determined by chiral HPLC analysis using commercially available columns.^c Reaction run at 0 °C.

Table 2

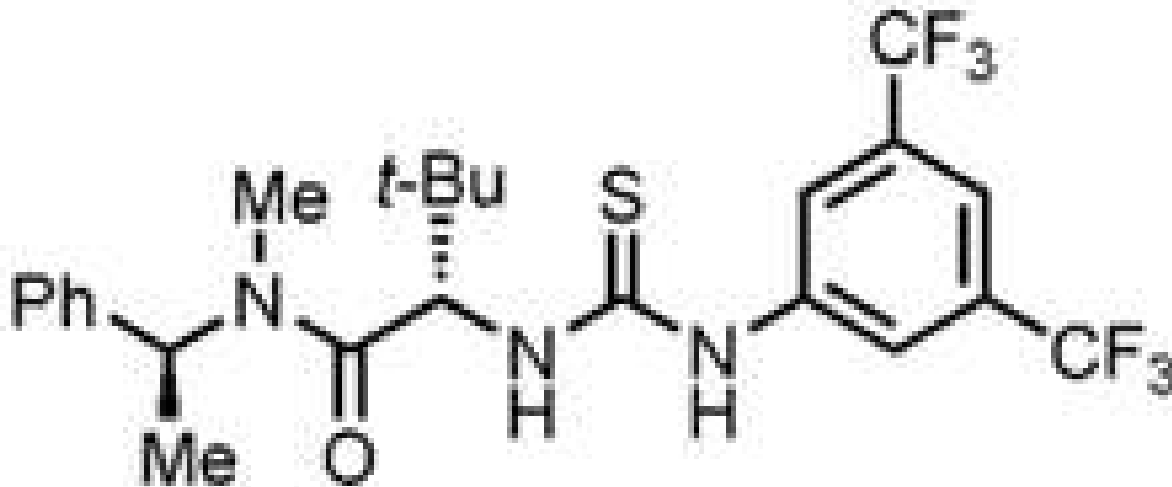
Correlation between catalyst structural properties and reaction rate and enantioselectivity in the hydrocyanation of **2a**

Entry	Catalyst	$k_{rel}^{a,b}$	$\Delta\Delta G^\ddagger$ (kcal/mol)	
1		1.0	47 ± 7	1.86 ± 0.0
2	<p>(4a)</p> 	0.1032 ± 6	1.67 ± 0.0	
3	<p>(6a)</p> 	0.1549 ± 2	1.88 ± 0.0	
4	<p>(7a)</p> 	0.6523.9 ± 0.4	1.53 ± 0.0	
5	<p>(4b)</p>  <p>(4c)</p> 	0.32	12.8 ± 0.2	1.23 ± 0.0

Entry Catalyst

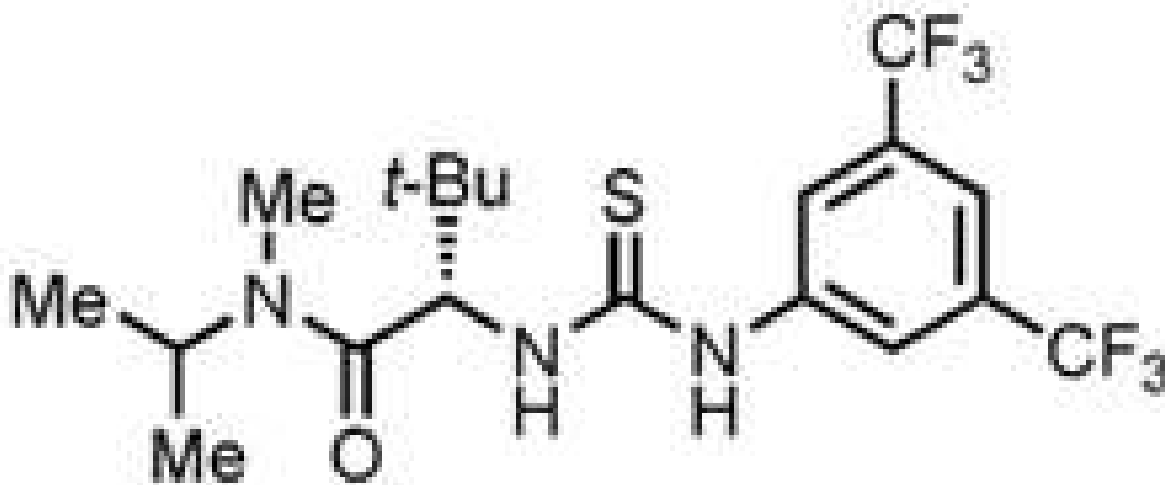
 k_{rel}^a er^b $\Delta\Delta G^\ddagger$ (kJ)

6

0.275.5 \pm 0.1 0.82 \pm 0.0

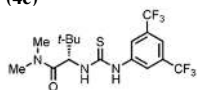
7

(4d)

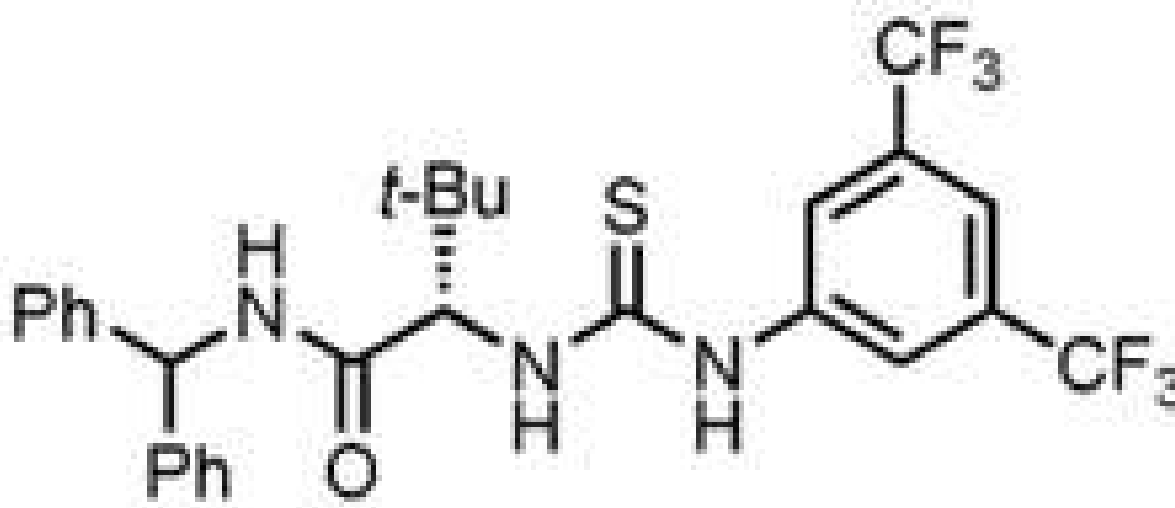
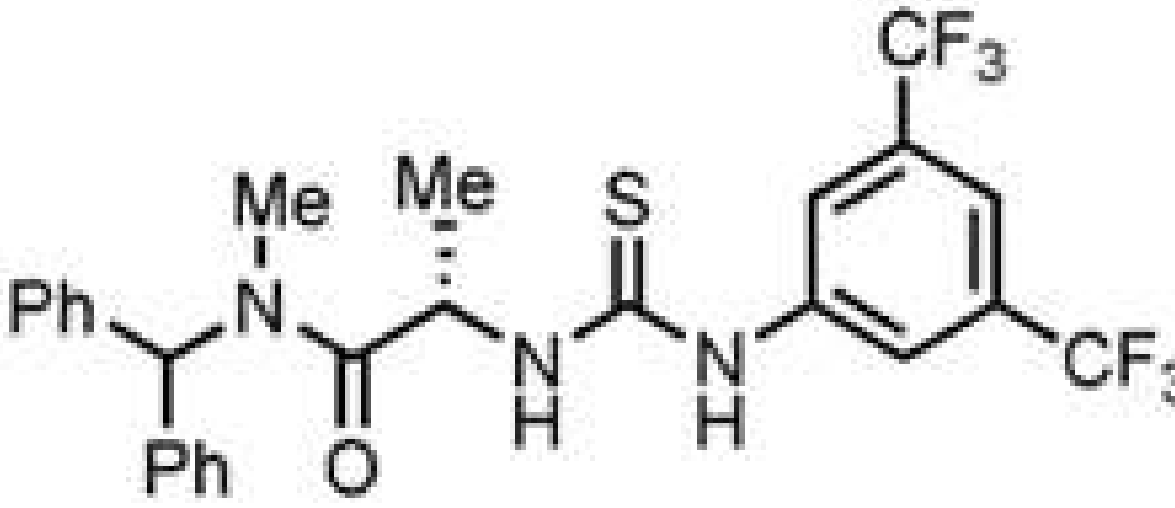
0.171.80 \pm 0.010.285 \pm 0.

8

(4e)

0.160.84 \pm 0.01-0.084 \pm 0.

(4f)

Entry	Catalyst	k_{rel}^a	$\Delta\Delta G^\ddagger$ (kJ/mol)
9		$0.426.00 \pm 0.040.865 \pm 0.0$	
10	<p>(4g)</p>  <p>(4h)</p>	$0.041.78 \pm 0.070.28 \pm 0.0$	

^aDetermined by in situ IR spectroscopy under pseudo-first order conditions: [imine]_i = 0.06 M, [TMSCN]_{tot} = 0.80 M, [MeOH] = 0.60 M, [cat]_{tot} = 0.006 M, toluene, 0 °C. Rate constants were determined by a fit to $f(x) = y_0 + ae^{k_{\text{obsd}}x}$, where x = absorbance.

^bDetermined by chiral HPLC analysis of isolated samples. Average of two independent experiments \pm 1 standard deviation. Conditions: -30 °C, 2 equiv TMSCN/MeOH, toluene (0.02 M), 14–20 h.

^cEstimated with $\Delta\Delta G^\ddagger = -R T \ln([R]/[S])$, T = 243.15.